AD_____

Award Number: DAMD17-01-1-0331

TITLE: Prediction of Chemotherapy Response by Magnetic Resonance Spectroscopy

PRINCIPAL INVESTIGATOR: Michael Garwood, Ph.D.

CONTRACTING ORGANIZATION: University of Minnesota
Minneapolis, MN 55455-2070

REPORT DATE: October 2004

TYPE OF REPORT: Final

PREPARED FOR: U.S. Army Medical Research and Materiel Command
Fort Detrick, Maryland 21702-5012

DISTRIBUTION STATEMENT: Approved for Public Release;
Distribution Unlimited

The views, opinions and/or findings contained in this report are those of the author(s) and should not be construed as an official Department of the Army position, policy or decision unless so designated by other documentation.

REPORT DOCUMENTATION PAGE

Form Approved
OMB No. 074-0188

1. AGENCY USE ONLY (Leave blank)	2. REPORT DATE	3. REPORT TYPE AND DATES COVERED
	October 2004	Final (17 Sep 2001 - 16 Sep 2004)

4. TITLE AND SUBTITLE
Prediction of Chemotherapy Response by Magnetic Resonance Spectroscopy

5. FUNDING NUMBERS
DAMD17-01-1-0331

6. AUTHOR(S)
Michael Garwood, Ph.D.

7. PERFORMING ORGANIZATION NAME(S) AND ADDRESS(ES)
University of Minnesota
Minneapolis, MN 55455-2070

E-Mail: gar@cmrr.umn.edu

8. PERFORMING ORGANIZATION REPORT NUMBER

9. SPONSORING / MONITORING AGENCY NAME(S) AND ADDRESS(ES)
U.S. Army Medical Research and Materiel Command
Fort Detrick, Maryland 21702-5012

10. SPONSORING / MONITORING AGENCY REPORT NUMBER

11. SUPPLEMENTARY NOTES

12a. DISTRIBUTION / AVAILABILITY STATEMENT
Approved for Public Release; Distribution Unlimited

12b. DISTRIBUTION CODE

13. ABSTRACT (Maximum 200 Words)

This research seeks to validate the use of MRS to assess therapeutic response in patients with locally-advanced breast cancer receiving primary systemic therapy (PST), or neoadjuvant chemotherapy. 35 women were enrolled in this study. Magnetic resonance spectroscopy (MRS) scanning was used to measure the tumor concentration of choline-containing compounds [tCho], which is known to be elevated in cancers and in proliferating cells. Clinical response was assessed by MRI measurements of tumor size based on the criteria of RECIST (response evaluation criteria in solid tumors). Changes in [tCho] between the baseline MRS scan (acquired <1 wk before starting PST) and that acquired 24 hours after the 1st dose of PST showed a significant positive correlation with change in tumor size measured after completing PST ($R=0.89$, $p<0.0001$). Opposite trends in [tCho] between objective responders and nonresponders ($p=0.0101$) were observed already at 24 hours after starting PST. These results show that MRS scanning can distinguish responders versus nonresponders early in the course of PST. These findings provide evidence that MRS may be used clinically to individualize treatments for maximizing benefit and to rapidly assess efficacy of new drugs. Findings are being published in *Radiology* in Fall 2004.

14. SUBJECT TERMS
magnetic resonance spectroscopy, metabolic imaging, chemotherapy

15. NUMBER OF PAGES
56

16. PRICE CODE

17. SECURITY CLASSIFICATION OF REPORT	18. SECURITY CLASSIFICATION OF THIS PAGE	19. SECURITY CLASSIFICATION OF ABSTRACT	20. LIMITATION OF ABSTRACT
Unclassified	Unclassified	Unclassified	Unlimited

Table of Contents

INTRODUCTION

Adjuvant chemotherapy reduces the risk of breast cancer death for essentially all stages of the disease, although the absolute benefits of chemotherapy are small. The development of many new effective agents may provide several improved options for many women. A major challenge in breast cancer treatment is to determine which chemotherapeutic agent will provide the most benefit for an individual patient. Effective chemotherapy inhibits cell proliferation and induces apoptosis. In previous studies of cells, it has shown that elevated levels of choline-containing compounds (tCho) are associated with proliferation (*1*), and that changes in cellular tCho levels occur during malignant transformation and progression (*2, 3*) and in altered resistance to chemotherapy (*4*). In vivo tumor concentrations of tCho, [tCho], can be measured non-invasively using in vivo magnetic resonance spectroscopy (MRS) and have been shown to be linked to malignant proliferation in brain tumors (*5*). The objective of this research is to determine whether in vivo MRS measurements of [tCho] can identify chemotherapy-induced growth arrest, and possibly apoptosis, in patients with locally-advanced breast cancer (LABC) who receive primary systemic therapy (PST), also known as neoadjuvant chemotherapy. The goal is to determine whether changes in [tCho] can identify responders and non-responders very early in the course of treatment (within 24 hr – 3 wks). The study employs a MR scanner having a high magnetic field (4 Tesla) which improves the sensitivity for [tCho] measurement. To measure tumor size changes and to locate the tumors for [tCho] measurements, the protocol also includes contrast-enhanced MRI scanning. MRS measurements of [tCho] are compared with clinical response based on tumor size changes by MRI and by pathological evaluation of the surgically-resected tissue after PST. This research is expected to show that MRS can be used to individualize and optimize adjuvant chemotherapy regimens for the treatment of breast cancer.

BODY

In the period of time since gaining approval by the HSRRB to use human subjects (January 2002), we enrolled 35 patients in the study and a total 179 MRS/MRI exams were performed on these subjects for the purpose of accomplishing Task 1: *Monitor changes in [tCho] by MRS and tumor size by MRI in response to PST.*

After completing data collection of the first 13 subjects who completed the full course of PST, we analyzed the data according to Task 2: *Determine how changes in MRS correlate with tumor response detected by MRI and with pathology findings.* The results are extremely exciting, since the MRS measured changes in [tCho] appear to predict clinical response consistently very early in the course of treatment. Because of the substantial correlation between changes in [tCho] with clinical response, we decided to report these novel findings before completing the planned accrual (see below). These findings are to be published in November 2004 (*6*) in an article entitled "Predicting Response to Neoadjuvant Chemotherapy of Locally Advanced Breast Cancer with In Vivo ^{1}H MRS: A Pilot Study at 4 Tesla". From the preprint of this article that is included in the Appendix, it can be seen that plots in figures 1, 3, and 5 show the most relevant data. As described in the article (*6*), changes in [tCho] between the baseline scan (acquired within 1 wk before starting PST) and 24 hours after the first cycle of PST

showed a significant positive correlation with change in tumor size (longest dimension, LD) after 4 cycles of doxorubicin-based PST ($R=0.79$, $p<0.001$). Opposite trends in [tCho] changes between objective responders and nonresponders ($p=0.0101$) were observed already by 24 hours after starting PST.

The total number of subjects studied (35) was less than the target number (77). We initially powered the study to detect changes in [tCho] sufficient to distinguish between patients achieving a pathological complete response from those with residual tumor left at definitive surgery. However, with the high accuracy of [tCho] to identify early response to PST, the projected sample size was not needed to accomplish the goals of this research. As described above, data obtained on the first 13 subjects already provided strong evidence of ability of MRS to identify early response to PST in patients with LABC. The presentation given at last year's RSNA meeting generated much interest among radiologists and oncologists in the field. We are currently getting inquiries about our study from breast cancer imagers and researchers from multiple institutions across the country. In late Summer 2004, a teleconference was organized to discuss the possibility of conducting a large multi-center clinical trial based on our pilot study. As a result, an initial application has recently been submitted to ACRIN (American College of Radiology Imaging Network), an agency that funds these types of large multi-center trials. We hope to be successful in obtaining funds so that the multi-center trial can begin before the end of 2005.

The MRS methodology used to quantify tCho in breast lesions is crucial to this project. Although the development of this methodology was not one of the specific Tasks in this project, the data generated as part of Task 1 could be used to help validate our tCho quantification procedure. An article describing our quantitative MRS methodology entitled "In Vivo Quantification of Choline Compounds in the Breast with 1H MR Spectroscopy" was published in 2003 (*7*) (see Appendix). In addition, in the process of conducting this research, we solved technical problems related to frequency shifts that previously degraded the quality of MR spectra of breast. This article is currently in press (*8*) (see Appendix).

KEY RESEARCH ACCOMPLISHMENTS

- We have shown that the concentration change of choline-containing compounds in the tumors (baseline versus 24 hours after the 1st cycle of chemotherapy) predicts clinical response (as determined by the change in tumor size measured by MRI; baseline versus 4 cycles of chemotherapy).
- These results suggest that MRS can be used clinically to distinguish responders versus nonresponders early in the course of neoadjuvant chemotherapy..

REPORTABLE OUTCOMES

Manuscripts:

S. Meisamy, P.J. Bolan, E.H. Baker, E. Gulbahce, L.I. Everson, M.T. Nelson, T. Emory, T. Tuttle, D. Yee, and M. Garwood, "Predicting Response to Neoadjuvant Chemotherapy

of the Locally Advanced Breast Cancer with In Vivo 1H MRS: A Pilot Study at 4 Tesla", *Radiology*, in press, 2004.

P.J. Bolan, S. Meisamy, E.H. Baker, J. Lin, T. Emory, M. Nelson, L.I. Everson, D. Yee, and M. Garwood, "In Vivo Quantification of Choline Compounds in the Breast with 1H MR Spectroscopy", *Magn. Reson. Med., 50*, 1134-1143, 2003.

Measurement and Correction of Respiration-Induced B_0 Variations in Breast ^{1}H MRS at 4 Tesla, P.J. Bolan, P.-G. Henry, E.H. Baker, S. Meisamy, and M. Garwood, *Magn. Reson. Med.*, in press, 2004.

Abstract and Presentation:

S. Meisamy, P.J. Bolan, J.C. Lin, L.I. Everson, M.T. Nelson, T. Emory, D. Yee, and M. Garwood, "The Value of Adding MRS to MRI for Predicting Response to Neoadjuvant Chemotherapy of Locally Advanced Breast Cancer: A Pilot Study at High Field", Annual Meeting of the RSNA, November 30 - December 5, 2003.
This abstract won the RSNA Research Trainee Award

Degree:

Funding from this grant provided salary support for a graduate student, Patrick Bolan, who completed his Ph.D. in December 2003. Dr. Bolan is currently a post-doctoral associate at the CMRR who continues to be focused on breast cancer research.

Personnel supported by this project:
Michael Garwood, Ph.D. (PI)
Douglas Yee, M.D. (Co-PI)
Michael Nelson, M.D. (Co-I)
Patrick Bolan, grad student (09/02-12/03), post-doc (01/04-09/04)

CONCLUSIONS

Clinical response can be predicted as early as 24 hours after the 1st cycle of doxorubicin-based chemotherapy using in vivo MRS measurement of choline-containing compounds in the tumor. These findings are highly significant because they show that MRS can distinguish responders versus nonresponders early in the course of treatment and suggest the use of MRS clinically to individualize treatments for maximizing benefit and to rapidly assess efficacy of new drugs.

REFERENCES

1. A. R. de Molina *et al.*, *Cancer Res* **64**, 6732-6739 (2004).
2. S. Singer, K. Souza, W. G. Thilly, *Cancer Res.* **55**, 5140-5145 (1995).
3. E. O. Aboagye, Z. M. Bhujwalla, *Cancer Res.* **59**, 80-84 (1999).
4. L. Le Moyec *et al.*, *Cancer Res.* **56**, 3461-3467 (1996).
5. S. Herminghaus *et al.*, *NMR Biomed.* **15**, 385-392 (2002).

6. S. Meisamy *et al.*, *Radiology* **in press** (2004).
7. P. J. Bolan *et al.*, *Magn Reson Med* **50**, 1134-1143 (2003).
8. P. J. Bolan, P.-G. Henry, E. H. Baker, S. Meisamy, M. Garwood, *Magn. Reson. Med.* **52**, 000-000 (2004).

APPENDICES

Attached

tapraid5/z3t-mrm/z3t-mrm/z3t01004/z3t1867d04a | heckt | S=7 | 8/26/04 | 8:41 | Art: 104-6985 | input-dp

Magnetic Resonance in Medicine 52:000–000 (2004)

Measurement and Correction of Respiration-Induced B_0 Variations in Breast ^{1}H MRS at 4 Tesla

Patrick J. Bolan,* Pierre-gilles Henry, Eva H. Baker, Sina Meisamy, and Michael Garwood

Respiratory motion is well known to cause artifacts in magnetic resonance spectroscopy (MRS). In MRS of the breast, the dominant artifact is not due to motion of the breast itself, but rather it is produced by B_0 field distortions associated with respiratory motion of tissues in the chest and abdomen. This susceptibility artifact has been reported to occur in the brain, but it is more apparent in the breast due to the anatomic proximity of the lungs. In the breast, these B_0 distortions cause shot-to-shot frequency shifts, which vary an average of 24 Hz during a typical ^{1}H MRS scan at 4 T. This variation can be corrected retrospectively by frequency shifting individual spectra prior to averaging. If not corrected, these shifts reduce spectral resolution and increase peak fitting errors. This work demonstrates the artifact, describes a method for correcting it, and evaluates its impact on quantitative spectroscopy. When the artifact is not corrected, quantification errors increase by an average of 28%, which dramatically impacts the ability to measure metabolite resonances at low signal-to-noise ratios. Magn Reson Med 52:000–000, 2004. © 2004 Wiley-Liss, Inc.

Key words: respiration; susceptibility; MRS; breast cancer

INTRODUCTION

Physiologic motion associated with respiratory and cardiac cycles is known to cause artifacts in magnetic resonance spectroscopy (MRS). The situation is most severe when the tissue being studied experiences gross motion, causing the voxel(s) to be displaced from the intended position. This is common in thoracic and abdominal MRS, where techniques such as triggering (1,2), breath-holding (3), and retrospective data rejection (4) can be used to reduce the impact of gross displacement. When motions are small relative to the voxel size, this displacement artifact is negligible. However, these small-scale motions can produce phase variations between consecutively acquired free induction decays (FIDs). If these are not corrected prior to averaging the FIDs, destructive interference will cause a decrease of signal intensities. These phase variations can be corrected by retrospectively phasing individual spectra prior to averaging. The reference for the phase correction can be derived from physiologic monitoring (5), from a navigator echo (6,7), or from resonances in the data itself (8–12). Alternatively, phase variations can be avoided altogether by using physiologic triggering (13).

MRS has been increasingly used in adjunct with breast MRI for diagnosing cancer and monitoring response to cancer treatments. Malignant breast lesions have been shown to contain elevated levels of choline-containing compounds, which appear as a single resonance at 3.2 ppm in ^{1}H MRS (14). Typical breast MRS studies are performed with the subject lying prone in the magnet and with a coil designed to support the breast. Consequently, motion of the breast tissue is restricted, and gross displacements are usually less than 1–2 mm. This motion produces the small edge artifacts that are commonly seen in subtraction images of dynamic contrast enhanced breast studies. Although these displacements are small compared to the typical ^{1}H MRS voxel size (~10 mm), they can still produce substantial phase variations.

Another effect of respiratory motion can occur even when the tissue within a voxel is completely immobile. As the lungs and diaphragm move during respiration, they create time-dependent B_0 variations that extend far from the chest (15,16). This was demonstrated by Raj et al., who showed that respiratory motion can produce significant signal fluctuations in EPI images acquired in a phantom placed adjacent to a subject's head (17). These B_0 fluctuations produce frequency shifts in acquired spectra. Previous studies in brain MRS have shown that this artifact degrades the quality of spectra averaged over multiple acquisitions by reducing spectral resolution and increasing quantitative fitting errors (11,12,18). In the brain, the magnitude of these shifts is on the order of 0.01 ppm, with reports of 0.3–2 Hz at 3 T (12,18) and 1.5–4 Hz at 7 T (16). These shifts are small relative to the spectral linewidth, so the spectral degradation caused by frequency shifts is a minor effect compared to the signal loss caused by phase variations (11). However, the magnitude of respiratory-induced B_0 shifts increases with proximity to the chest (16,19). As is demonstrated in this work, the magnitude of these shifts in the breast is typically 0.1 ppm—10× greater than that measured in the brain.

This article aims to measure this artifact and evaluate its impact on quantitative breast MRS. Breath-hold imaging and physiologic monitoring were used to determine the relationship between MRS frequency shifts and respiration. Spectral fitting and quantification were performed both with and without retrospective frequency correction to demonstrate that fitting errors decrease significantly when frequency correction is performed.

METHODS

All measurements were performed with a research 4-T system, consisting of a 90-cm bore magnet (model 4 T-900,

Center for Magnetic Resonance Research and Department of Radiology, University of Minnesota School of Medicine, Minneapolis, Minnesota

Presented in part at 2002 ISMRM Annual Meeting, Honolulu, Hawaii. Grant sponsors: NIH Grants RR08079, CA92004, RR00400, and CA77398; DOD Breast Cancer Research program DAMD 17-01-1-0331; Lillian Quist-Joyce Henline Chair in Biomedical Research; University of Minnesota Doctoral Dissertation Fellowship

* Correspondence to: Patrick J. Bolan, Ph.D., Center for Magnetic Resonance Research, 2021 Sixth Street SE, Minneapolis, MN 55455. E-mail: bolan@cmrr.umn.edu

Received 31 March 2004; revised 24 June 2004; accepted 30 June 2004

DOI 10.1002/mrm.00000

Published online in Wiley InterScience (www.interscience.wiley.com).

Oxford Magnet Technology, Oxfordshire, UK) with a clinical gradient system (Model Sonata, Siemens, Erlangen, Germany) interfaced with an imaging spectrometer (Model Unity Inova, Varian, Palo Alto, CA). Several different single-breast quadrature transmit/receive RF surface coils of similar design were used to accommodate different breast sizes (20). The coils were mounted onto a custom-built patient table designed for unilateral, prone breast studies. In several examinations, a pneumatic belt was wrapped around the thorax just below the breasts to acquire chest expansion data. The subject population for this study included both normal volunteers and patients with either a suspicious breast lesion or a known breast cancer. The study was approved by our institutional review board, and informed consent was obtained prior to performing each experiment. All processing of images and spectra was performed using Matlab (The Mathworks, Natick, MA).

Assessment of Respiratory Effects

Breath-hold imaging was performed in three normal subjects to evaluate the spatial variation of respiration artifacts. Single-slice gradient echo images (matrix = 256 × 128, slice thickness = 5 mm, field of view = 14 cm, TR/TE = 50/15 ms) were acquired during breath holds at both maximum inspiration and maximum expiration. Maps of the phase difference ($\Delta\ddot{o}$) between inspiration and expiration were created by dividing the two complex images and extracting the phase. A mask for the high signal-to-noise region was created by thresholding the magnitude image and applying spatial smoothing (using Matlab's *bwmorph* function). The $\Delta\ddot{o}$ map was smoothed (median filter, 8 × 8 kernel) and manually unwrapped to correct phase discontinuities greater than π. The $\Delta\ddot{o}$ map was then converted into a frequency-shift map $\Delta\nu = \Delta\ddot{o}/(2\pi TE)$, expressed in hertz.

Spectroscopy Acquisition

In vivo spectra were recorded as part of our standard breast MR protocol, consisting of a dynamic contrast-enhanced MRI study followed by single-voxel spectroscopy. After localized shimming and power calibration, single-voxel spectra were acquired using localization by adiabatic selective refocusing (LASER) (21). Water suppression was performed using variable pulse power and optimized relaxation delays (VAPOR) (22). TE averaging (23) was used to reduce lipid sideband artifacts (TE = 45–196 ms in N = 64 or 128 increments, TR = 3 s). Each FID was individually saved—no averaging was performed until processing. A fully relaxed, single-shot spectrum with no water suppression was also acquired from each voxel to provide a reference water resonance.

Postprocessing

Spectra were postprocessed and the levels of total choline-containing compounds (tCho) were calculated using a fully automated method described previously (14) and summarized briefly here. For postprocessing, each individually saved FID was automatically corrected for DC offset and variation of zero-order phase. Frequency shifts between individual FIDs were calculated using a frequency-domain cross-correlation method (18). Each FID was shifted in frequency by multiplying the time-domain data by a linear phase function, $\exp(I \cdot 2\pi \cdot \Delta\nu \cdot t)$. The frequency shift magnitude $\Delta\nu$ was chosen to maximize the cross-correlation (evaluated in modulus mode and in the frequency domain) between the spectrum and a reference spectrum (arbitrarily, the first in the series). The variability of $\Delta\nu$ over all FIDs in a single-voxel acquisition was characterized by its range $R(\Delta\nu)$ and SD $\sigma(\Delta\nu)$.

The quantification method used the unsuppressed water resonance as an internal reference to normalize the amplitude of the tCho resonance and obtain an estimate of the concentration (denoted [tCho]) expressed in molal units (mmol/kg-water). Spectral fitting was performed one resonance at a time by fitting a Voigt line shape to a narrow band of the frequency domain (0.4 ppm) centered around the resonance. The fitting error (i.e., the measurement uncertainty) was estimated using the Cramér–Rao minimum variance bound, which was calculated using the covariance matrix provided by the fitting routine. The SD of the fitting error, σ_{tCho}, was normalized to the amplitude of the tCho resonance and expressed as a percentage. This error was also used to establish the detectability threshold as follows: if σ_{tCho} was greater than 100% then the tCho resonance was considered undetectable.

Quantitative Spectroscopy

A retrospective analysis was performed to evaluate whether the frequency correction impacts the results of spectral quantification. In vivo breast MRS data acquired from subjects over a 2-year period were included in this study. The subjects included 21 patients with biopsy-confirmed cancer undergoing neoadjuvant chemotherapy, 46 patients with a suspicious breast lesion evaluated immediately pre- or postbiopsy, and 5 normal volunteers. A total of 715 TE-averaged spectra were acquired from all 72 subjects in 140 studies. A subset of 280 spectra were chosen for this retrospective analysis by removing 9 spectra with visible artifacts, 151 spectra with lipid content greater than the previously specified threshold (14), and 275 spectra with no detectable tCho resonance. These 280 spectra were processed and quantified both with and without frequency correction. Omission of the frequency correction step is equivalent to the common practice of automatically averaging FIDs prior to postprocessing.

RESULTS

Assessment of Respiratory Effects

Figure 1 is a representative data set showing sagittal images from one breath-hold study of a normal breast. Magnitude images acquired during maximum inspiration (Fig. 1a) and maximum expiration (Fig. 1b) are very similar. The magnitude difference image (Fig. 1c) shows that the gross motion of the breast was small during respiration, causing only small edge artifacts. The phase difference between inspiration and expiration was converted into a map of frequency shift, $\Delta\nu$, shown in Fig. 1 day. The $\Delta\nu$ map shows a strong spatial dependence, with the greatest effect (~70 Hz) closest to the chest wall. A voxel placed in the center of the breast would have experienced a shift of

F1

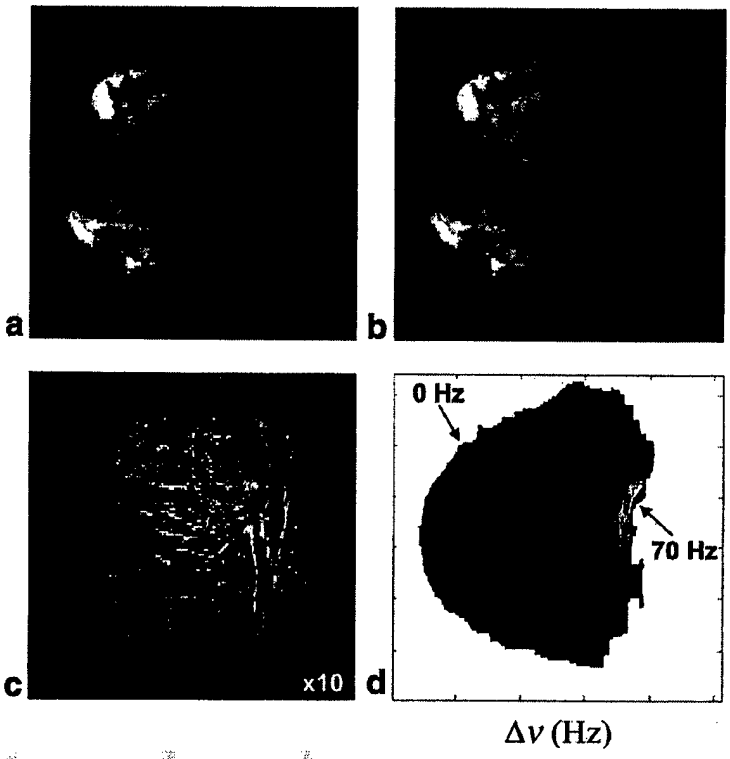

FIG. 1. Demonstration of respiration artifacts by MR imaging. The top row shows sagittal gradient-echo images of a subject's left breast during breath-holds at (a) maximum inspiration and (b) maximum expiration. The magnitude difference between these two images is shown in **c**, scaled by a factor of 10, showing that there was little gross motion of the breast during respiration. The phase difference between **a** and **b** was converted into a $\Delta\nu$ map, shown in **d**, with contour lines every 10 Hz. The frequency shift varied from <10 Hz at the skin to 70 Hz nearest the chest wall.

10–20 Hz between maximum inspiration and expiration. Similar $\Delta\nu$ maps were reproduced in each breath-hold subject. The largest frequency shifts were nearest the chest wall in both left and right breasts and in axial and sagittal orientations.

The relationship between MRS frequency shifts and the F2 respiratory cycle is shown in Fig. 2. In the figure, the dots indicate frequency shifts measured from NMR spectra using the cross-correlation method described above. The line shows the chest expansion measured by the pneumatic belt, scaled and shifted to match the frequency shifts. The good agreement between these data sets indicates that the frequency shifts were most likely caused by respiration rather than by cardiac motion. This also suggests that physiologic monitoring of the chest expansion could be used to correct frequency shifts in the spectra.

Frequency Correction Examples

The frequency correction method is demonstrated in Fig. F3 3, which shows a series of single-shot (NEX = 1), fixed TE (TE = 45 ms) spectra acquired from a malignant lesion. The frequency variation evident in the uncorrected spectra (Fig. 3a) is removed after frequency correction (Fig. 3b). After averaging and fitting both the corrected and uncor- F4 rected series, the corrected spectrum (Fig. 4a, top) had improved spectral resolution, increased tCho amplitude, and decreased fitting error as compared to the uncorrected spectrum (Fig. 4a, bottom). This example is not representative of a typical acquisition, because the SNR was atypically high and TE averaging was not used. However, this case provides a clear example of the impact of the frequency correction method.

Several representative examples of TE-averaged acquisitions are shown in Figs. 4b–d, with and without fre-

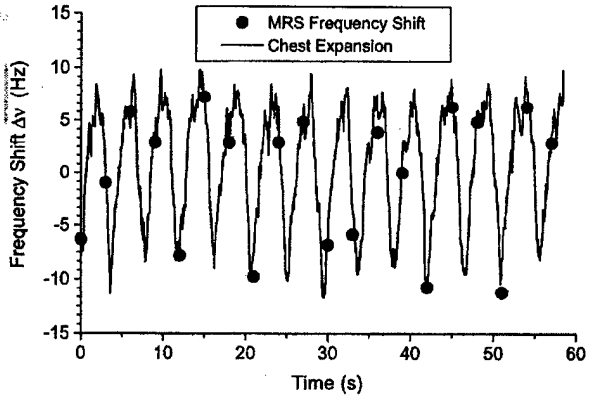

FIG. 2. Demonstration of the relationship between spectral frequency shifts and chest expansion. The subject was asked to breathe normally while a series of localized, unsuppressed spectra were acquired with TR = 3 s. The line shows the (smoothed) chest expansion as measured with a pneumatic chest bellows. The dots show the magnitude of frequency shifts measured using the cross-correlation method on the spectra at corresponding time points. The magnitude of the chest expansion data were manually scaled to match the measured frequency offsets.

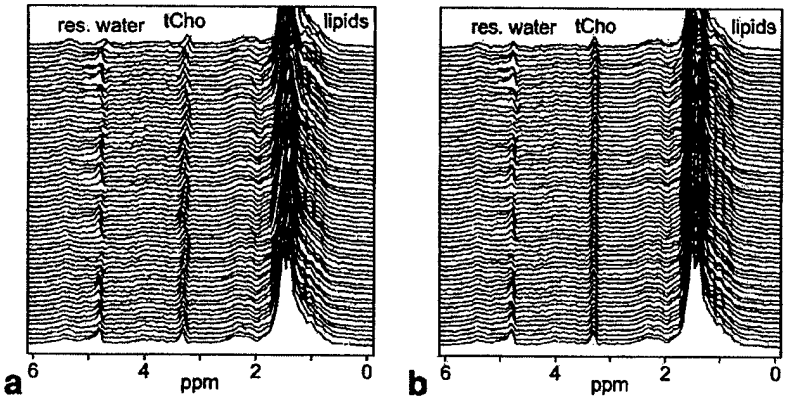

FIG. 3. Demonstration of frequency correction. A series of 64 identical single-shot (NEX = 1), water-suppressed, in vivo spectra (TR/TE = 3000/45 msec) acquired during normal respiration are shown (a) prior to and (b) after frequency correction using the cross-correlation method. The measured frequency shifts in this acquisition varied over a range of $R(\Delta\nu)$ with a SD of $\sigma(\Delta\nu)$. Note that these data are not TE-averaged and have an unusually high signal-to-noise ratio.

quency correction. Figures 4b and 4c show how the magnitude of the frequency variation can affect the spectral quality. Both are good-quality spectra with resonance from several metabolites in addition to tCho. In Fig. 4b, the corrected and uncorrected spectra appear similar because the frequency variation was relatively small. In Fig. 4c, where the frequency variation was larger, the corrected data clearly show improved spectral resolution. Fig. 4 days shows a case where tCho was detectable with frequency correction and not detectable (using the σ_{tCho} criterion) when the frequency correction was omitted.

Quantitative Spectroscopy

The quantification procedure was performed using frequency correction on the full set of 280 TE-averaged spectra with a detectable tCho resonance. These spectra were then reprocessed with the frequency correction step removed. The resultant spectral broadening generally increased the Cramér–Rao errors, making the tCho resonance undetectable in 69/280 (25%) spectra based on the $\sigma_{tCho} < 100\%$ criterion. Of the remaining 211 spectra, the calculated [tCho] values, shown in Fig. 5a, did not change ($P =$ 0.28, two-tailed t test). The errors, shown in Fig. 5b, were an average of 28% larger when the frequency correction was omitted. As expected, the increase in error was greater when the magnitude of the frequency variation was larger, as shown in Fig. 5c. The range and SD of the frequency variation are shown as histograms in Fig. 5 days. The mean range of the frequency variation $R(\Delta\nu)$ was 24 Hz (0.14 ppm). F5

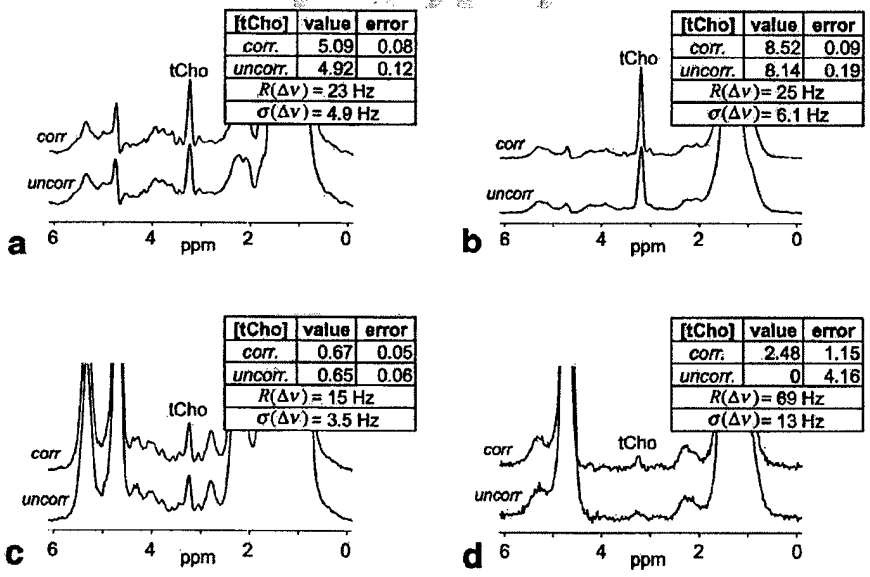

FIG. 4. Impact of frequency correction on spectral quantification. Each pair of spectra shown in **a–d** are averaged from the same acquired data but processed with (top) and without (bottom) frequency correction. The inset tables show calculated [tCho] concentrations and fitting errors (mmol/kg) based on the method in Ref 14 for both corrected an uncorrected spectra. The range $R(\Delta\nu)$ and SD $\sigma(\Delta\nu)$ of the frequency variation over each acquisition is also shown. The pair in **a** are averaged from the single-TE arrays shown in Figs. 3(**a**) and (**b**). Pairs **b–d** are examples of TE-averaged spectra (TE = 45–196 ms in 128 increments, TR = 3 s), demonstrating cases where the effect of frequency correction is relatively small (**b**), moderate (**c**), and large (**d**). In the uncorrected spectrum of **d**, the normalized fitting error (σ_{tCho} = 140%) exceeded the detection threshold, so in this case a tCho resonance is only detectable with frequency correction.

tapraid5/z3t-mrm/z3t-mrm/z3t01004/z3t1867d04a | heckt | S=7 | 8/26/04 | 8:41 | Art: 104-6985 | Input-dp

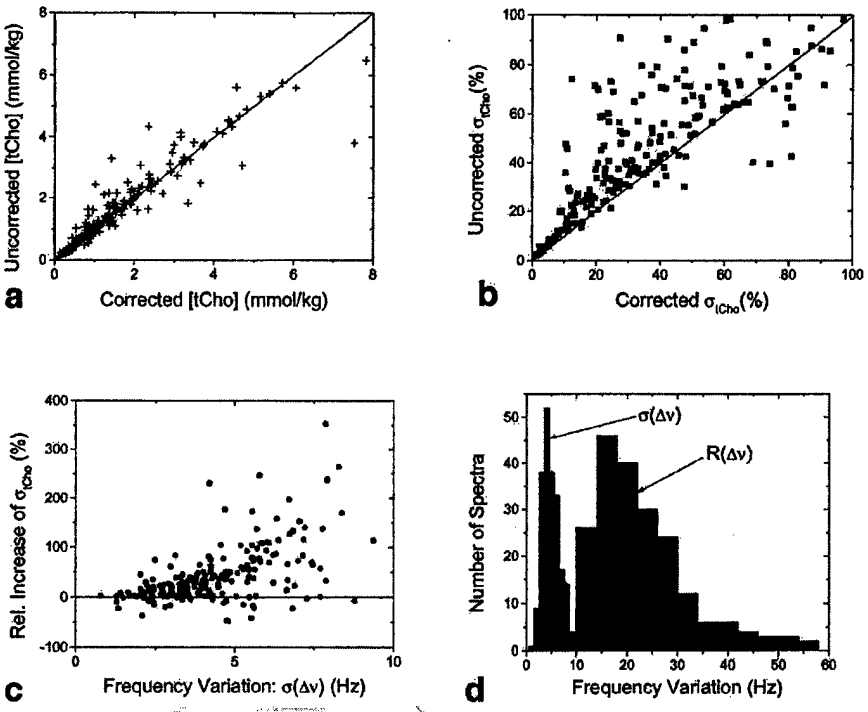

FIG. 5. Quantitative impact of frequency correction on quantification error evaluated in a series of 280 in vivo spectra. (a) Plot compares the total tCho concentration ([tCho]) when processed with and without frequency correction. There is no significant difference ($P = 0.28$). (b) Plot shows the fitting errors (normalized SD based on Cramér–Rao lower bounds) when processed with and without frequency correction. On average, the error is 28% larger without frequency correction. (c) The increase in error is plotted against the SD of $\Delta\nu$ for each spectrum. (d) Histograms for the range $R(\Delta\nu)$ and SD $\sigma(\Delta\nu)$ of the frequency variation in all 280 spectra.

DISCUSSION

This study demonstrates that the correction of respiratory-induced frequency variations improves the quality of breast ^1H MRS at 4 T. The proposed method of retrospectively correcting frequency shifts prior to averaging is applicable in cases where gross displacement of the tissue is relatively small, but B_0 variations are substantial. This scenario is typical of high-field breast MRS, in which breast motion is restricted by the coil platform, but frequency variations are large due to the proximity of the lungs. These frequency variations will be greater at higher magnetic fields because susceptibility-induced field distortions scale with field strength. The impact of this artifact has not been reported at 1.5 T, presumably because the susceptibility effects are less apparent than at 4 T.

The magnitude of the respiration-induced frequency variation measured in the breast at 4 T typically ranges from 10 to 30 Hz, with a mean of 24 Hz found in this study. The magnitude depends on the position of the voxel within the breast. All the $\Delta\nu$ maps acquired in this study showed a general trend of increased frequency variation closer to the chest wall. Further studies are required to measure the full spatial dependence of $\Delta\nu$ and determine if cardiac motion contributes to the effect. Other factors not explicitly measured but expected to affect the artifact include depth of respiration, chest size, and body composition. If left uncorrected, frequency variations during an acquisition will cause a blurring of the averaged spectrum, reducing the effective spectral resolution and distorting the line shape.

Although the qualitative impact of frequency shifts on breast spectra is often not dramatic, particularly when the frequency shifts are small, the quantitative impact of this artifact is always present. Even small frequency variations produce an increase in fitting errors (Fig. 5c), effectively decreasing the sensitivity of spectroscopic measurements. This is most critical when fitting metabolites at low signal-to-noise ratios, which is common in breast MRS.

The increased error is likely explained by the increased line widths produced by uncorrected frequency variation. In general, peak amplitude estimation errors are larger for broader resonances. This has been shown analytically for the case of a simple Lorentzian resonance (24). The Voigt line-shape model used in this work is equivalent to a Lorentzian line shape convolved with a Gaussian frequency blurring, which enables the model to account for frequency variations without introducing bias in the amplitude estimates. These properties were verified by simulating spectral data sets with random frequency variations: as the magnitude of frequency variation increased, the amplitude estimates did not change, but the amplitude *error* estimates did increase (data not shown). These results are consistent with the in vivo data shown in Fig. 5a–c. Although not evaluated in this work, it is expected that other spectral fitting methods would produce similar results, provided a sufficiently flexible line-shape model is used. This is supported by a previous study (11) that showed an increase in fitting errors but no affect on peak amplitudes when fitting spectra with the LCModel software package (25), which also uses a flexible line-shape model.

There are a number of approaches for handling respiration-induced frequency variations. In principle, the artifact can be avoided altogether using respiratory triggering

or breath-hold acquisitions. These methods are error-prone and are less efficient in use of machine time, but are necessary for spectroscopic editing techniques requiring precise frequency selectivity. Alternatively, the frequency distortion function $\Delta\nu(t)$ can be estimated and retrospectively corrected prior to averaging spectra, as is commonly done for phase variations. The $\Delta\nu(t)$ function can be estimated from either physiologic monitoring, MR navigator signals, or directly from the acquired data. Physiologic monitoring, typically done with chest expansion bellows or ECGs, is least direct and requires careful processing to properly denoise and detrend the data. Using navigator signals has the disadvantage that there is typically a delay between the navigator acquisition and the actual FID; the length of the delay may be significant when compared to the respiratory period. Although not shown, we also developed and tested a version of LASER with an interleaved small-flip-angle STEAM acquisition immediately following the metabolite acquisition period, similar to the method described by Thiel et al. (7). This also worked acceptably, but it was not as effective as the cross-correlation method, probably due to the delay between the navigator echo and the measured FID (350 ms). A nonlocalized navigator with a shorter delay was also tested, but these shift measurements did not correlate well with the localized shifts.

Extracting $\Delta\nu(t)$ directly from the data, as in this work, is the most direct way of measuring the artifact. This approach requires sufficient SNR in each acquisition to measure frequency shifts. Numerous methods have been proposed for measuring $\Delta\nu$ between consecutive spectra, including cross-correlation, frequency-referencing a single resonance, time domain fitting, and principal component analysis (18,26). The time domain method does not work well with TE-averaged data because the initial portion of each individual FID is distorted by B_0 modulations, which are corrected only after averaging. The single resonance referencing method (with the 1.3-ppm lipid) and cross-correlation method worked comparably, but the cross-correlation method was overall more robust because it uses the full spectral information. Using the residual water resonance as a frequency reference has been proposed by other groups (10,12). This approach is also feasible provided the water suppression is adjusted properly and has sufficient bandwidth to avoid frequency-dependent lineshape variations like those shown in Fig. 3a. Methods using principle component analysis may also be effective, but their applicability for TE-averaged spectra has not yet been investigated.

This study did not measure spectroscopic phase variations due to physiologic motion. Although in studies of compliant subjects there were generally no large-scale motions of the breast, small displacements of the breast (particularly near the chest wall) were visible by imaging. These small-scale breast motions may produce phase variations (10). With the TE-averaged acquisition method used in this work, the zero-order phase varies with each TE due to B_0 modulations, so phase correction is required even in the absence of motion. Therefore, separating physiologic and system sources of phase variation was not feasible.

CONCLUSION

This study reports measurements of respiratory-induced frequency variations in the breast at 4T and their impact on quantitative MRS. The average frequency variation measured over a typical acquisition was 24 Hz, which is approximately 10× greater than comparable measurements of this effect in the brain. If left uncorrected, this artifact reduces the ability to measure metabolite concentrations. In our sample of 280 spectra with a detectable tCho resonance, quantitative fitting errors increased by an average of 28%, and in 69 (25%) spectra the tCho resonance became undetectable. These results indicate that using frequency correction can improve the quality of quantitative breast ^{1}H MRS at high field.

REFERENCES

1. Dixon RM, Frahm J. Localized proton MR spectroscopy of the human kidney in vivo by means of short echo time STEAM sequences. Magn Reson Med 1994;31(5):482–487.
2. Felblinger J, Jung B, Slotboom J, Boesch C, Kreis R. Methods and reproducibility of cardiac/respiratory double-triggered 1H-MR spectroscopy of the human heart. Magn Reson Med 1999;42(5):903–910.
3. Katz-Brull R, Rofsky NM, Lenkinski RE. Breathhold Abdominal and Thoracic Proton MR Spectroscopy at 3T. Magn Reson Med 2003;50: 461–467.
4. Tyszka JM, Silverman JM. Navigated single-voxel proton spectroscopy of the human liver. Magn Reson Med 1998;39(1):1–5.
5. Felblinger J, Kreis R, Boesch C. Effects of physiologic motion of the human brain upon quantitative 1H-MRS: analysis and correction by retro-gating. NMR Biomed 1998;11(3):107–114.
6. Posse S, Cuenod CA, LeBihan D. Motion artifact compensation in 1H spectroscopic imaging by signal tracking. J Magn Reson B 1993;102: 222–227.
7. Thiel T, Gzisch M, Elbel GK, Hennig J. Phase coherent averaging in magnetic resonance spectroscopy using interleaved navigator scans: compensation of motion artifacts and magnetic field instabilities. Magn Reson Med 2002;47(6):1077–1082.
8. Zhu G, Gheorghiu D, Allen PS. Motional degradation of metabolite signal strengths when using STEAM: a correction method. NMR Biomed 1992;5(4):209–211.
9. Ziegler A, Decorps M. Signal-to-noise improvement in in vivo spin-echo spectroscopy in the presence of motion. J Magn Reson B 1993; 102:26–34.
10. Star-Lack JM, Adalsteinsson E, Gold GE, Ikeda DM, Spielman DM. Motion correction and lipid suppression for 1-H magnetic resonance spectroscopy. Magn Reson Med 2000;43:325–330.
11. Helms G, Piringer A. Restoration of motion-related signal loss and line-shape deterioration of proton MR spectra using the residual water as intrinsic reference. Magn Reson Med 2001;46(2):395–400.
12. Katz-Brull R, Lenkinski RE. Frame-by-frame PRESS 1H-MRS of the brain at 3 T: the effects of physiological motion. Magn Reson Med 2004;51(1):184–187.
13. Pattany PM, Khamis IH, Bowen BC, Goodkin K, Weaver RG, Murdoch JB, Donovon Post MJ, Quencer RM. Effects of physiologic human brain motion on proton spectroscopy: quantitative analysis and correction with cardiac gating. Am J Neuroradiol 2002;23(2):225–230.
14. Bolan PJ, Meisamy S, Baker EH, Lin J, Emory T, Nelson M, Everson LI, Yee D, Garwood M. In vivo quantification of choline compounds in the breast with 1H MR spectroscopy. Magn Reson Med 2003;50:1134–1143.
15. Noll DC, Schneider W. Respiration artifacts in functional brain imaging: sources of signal variation and compensation strategies. In: Proceedings of the 2nd Annual Meeting of SMR, San Francisco, 1994. p 647.
16. Van de Moortele PF, Pfeuffer J, Glover GH, Ugurbil K, Hu X. Respiration-induced B0 fluctuations and their spatial distribution in the human brain at 7 Tesla. Magn Reson Med 2002;47(5):888–895. AQ: 1
17. Raj D, Anderson AW, Gore JC. Respiratory effects in human functional magnetic resonance imaging due to bulk susceptibility changes. Phys Med Biol 2001;46(12):3331–3340.

18. Henry P-G, van de Moortele P-F, Giacomini E, Nauerth A, Bloch G. Field-frequency locked in vivo proton MRS on a whole-body spectrometer. Magn Reson Med 1999;42(4):636–642.
19. Raj D, Paley DP, Anderson AW, Kennan RP, Gore JC. A model for susceptibility artefacts from respiration in functional echo-planar magnetic resonance imaging. Phys Med Biol 2000;45(12):3809–3820.
20. Merkle H, DelaBarre L, Bolan PJ, Baker EH, Everson LI, Yee D, Garwood M. Transceive quadrature breast coils and applications at 4 Tesla. In: Proceedings of the 9th Annual Meeting of ISMRM, Glasgow, 2001. p 1114.
AQ: 2 21. Garwood M, DelaBarre L. The return of the frequency sweep: designing adiabatic pulses for contemporary NMR. J Magn Reson 2001;153(2): 155–177.
22. Tkac I, Starcuk Z, Choi IY, Gruetter R. In vivo 1H NMR spectroscopy of rat brain at 1 msec echo time. Magn Reson Med 1999;41:649–656.
23. Bolan PJ, DelaBarre L, Baker EH, Merkle H, Everson LI, Yee D, Garwood M. Eliminating spurious sidebands in 1-H MRS of breast lesions. Magn Reson Med 2002;48(2):215–222.
24. Yao Y-X, Pandit SM. Cramer–Rao lower bounds for a damped sinusoidal process. IEEE Trans Signal Proc 1995;43(4):878–885.
25. Provencher SW. Estimation of metabolite concentrations from localized in vivo proton NMR spectra. Magn Reson Med 1993;30(6):672–679.
26. Brown TR, Stoyanova R. NMR Spectral quantitation by principal-component analysis. II. Determination of frequency and phase shifts. J Magn Reson B 1996;112:32–43.

Magnetic Resonance in Medicine 50:1134–1143 (2003)

In Vivo Quantification of Choline Compounds in the Breast With ^{1}H MR Spectroscopy

Patrick J. Bolan,[1,2] Sina Meisamy,[1,2] Eva H. Baker,[1,2] Joseph Lin,[1,2] Timothy Emory,[2] Michael Nelson,[2] Lenore I. Everson,[2] Douglas Yee,[3,4] and Michael Garwood[1–3*]

This work describes a methodology for quantifying levels of total choline-containing compounds (tCho) in the breast using in vivo ^{1}H MR spectroscopy (MRS) at high field (4 Tesla). Water is used as an internal reference compound to account for the partial volume of adipose tissue. Peak amplitudes are estimated by fitting one peak at a time over a narrow frequency band to allow measurement of small metabolite resonances in spectra with large lipid peaks. This quantitative method significantly improves previously reported analysis methods by accounting for the variable sensitivity of breast ^{1}H MRS measurements. Using this technique, we detected and quantified a tCho peak in 214 of 500 in vivo spectra. tCho levels were found to be significantly higher in malignancies than in benign abnormalities and normal breast tissues, which suggests that this technique could be used to diagnose suspicious lesions and monitor response to cancer treatments. Magn Reson Med 50: 1134–1143, 2003. © 2003 Wiley-Liss, Inc.

Key words: choline; breast cancer; quantification; MRS; diagnosis

Breast cancer is a very common disease, affecting 11% of American women and causing more than 40000 deaths each year (1). While breast cancer mortality is decreasing, the incidence continues to rise (2). Thus, there is a great need for noninvasive diagnostic tools for both screening and treatment monitoring. The conventional diagnostics—X-ray mammography, sonography, and physical examination—are limited in their sensitivity for detecting disease and their specificity for distinguishing between benign and malignant lesions. Magnetic resonance imaging (MRI) of the breast is being used increasingly because of its high sensitivity, but its reported specificity is widely variable (3).

Researchers have recently begun to augment breast MRI studies with MR spectroscopy (MRS) to increase specificity. In vivo MRS can detect a resonance at 3.25 ppm that has contributions from several different compounds, including choline, phosphocholine, glycerophosphocholine, and taurine. High-resolution in vitro and ex vivo studies indicate that the levels of choline compounds increase with malignancy (4–6). At the lower field strengths used for in vivo work (1.5–4 T), these multiple resonances cannot be spectrally resolved and thus appear as a single peak, termed total choline-containing compounds (tCho).

Several studies conducted at 1.5 T have shown that in vivo MRS can be used to distinguish between benign and malignant tissues (7–11). These studies used the hypothesis that tCho is only detectable in malignancies. A pooled analysis of these five studies showed that this tCho detectability criterion can identify malignancies with an 83% sensitivity and 85% specificity (12). This qualitative approach is promising, but it is only applicable if the MRS measurement sensitivity is invariant. In similar studies performed at 4 T, the increased sensitivity allows detection of tCho in benign lesions and normal subjects. A more general approach is to quantify the tCho peak with the expectation that tCho levels are higher in malignancies than in benign lesions or normal tissues. Two groups have reported quantification of tCho levels using external phantom referencing methods (7,13). These studies demonstrated the feasibility of quantitative breast MRS, but they were limited to small patient groups and did not report measurement errors. Quantification is also valuable for measuring tumor response to treatment regimens. Two other studies found that the detectability and amplitude (judged qualitatively) of the tCho peak decreases after chemotherapy (8,11). A quantitative method enables finer measurements of the magnitude and rate of tumor response.

Although quantification of metabolite levels is routinely performed in MRS of the brain, it is more difficult to perform in the breast because of the heterogeneous distribution of the glandular and adipose tissues. Although the spectroscopist will typically plan a voxel to include mainly glandular tissue and tumor, voxels of typical size (1–2 mL) nearly always contain some adipose tissue as well. The amount of included adipose tissue can vary greatly depending on the architecture of the gland and/or lesion.

The two basic elements of a quantitative MRS methodology are the referencing strategy and the spectral fitting technique. The referencing strategy proposed in this work uses water as an internal reference peak. This approach compensates for the partial volume of adipose tissue in the voxel and naturally leads to a molal (mol/kg) concentration for water-soluble metabolites. The fitting technique used in this work is based on a hybrid time-domain (TD)

[1]Center for Magnetic Resonance Research, University of Minnesota School of Medicine, Minneapolis, Minnesota.
[2]Department of Radiology, University of Minnesota School of Medicine, Minneapolis, Minnesota.
[3]Cancer Center, University of Minnesota School of Medicine, Minneapolis, Minnesota.
[4]Department of Medicine, University of Minnesota School of Medicine, Minneapolis, Minnesota.

Presented in part at the ISMRM Workshop on In Vivo Functional and Molecular Assessment of Cancer, Santa Cruz, 2002 (for which the first author received the Negendank Award).

Grant sponsor: NIH; Grant numbers: RR08079; CA92004; RR00400; CA77398; Grant sponsor: DOD Breast Cancer Research Program; Grant number: DAMD 17-01-1-0331; Grant sponsor: Tickle Family Land Grant Endowment in Breast Cancer Research.

*Correspondence to: Michael Garwood, Ph.D., Center for Magnetic Resonance Research, 2021 Sixth St. SE, Minneapolis, MN 55455. E-mail: gar@cmrr.umn.edu

Received 8 May 2003; revised 11 August 2003; accepted 13 August 2003.
DOI 10.1002/mrm.10654
Published online in Wiley InterScience (www.interscience.wiley.com).

and frequency- domain (FD) method called "TDFD fitting" (14). This method enables flexible lineshape definition by the use of a TD model, and has excellent frequency-selection properties since the residuals are evaluated and minimized in the FD. The ability to select a narrow frequency range is crucial for fitting small resonances in the presence of very large ones, as is the case in breast spectra containing large lipid peaks.

The goal of this project was to develop a method to quantitatively measure tCho levels in breast tissue. The methodology presented integrates several existing techniques: single-voxel localization by adiabatic selective refocusing (LASER) (15), TE averaging to reduce lipid sideband artifacts (16), automatic frequency referencing to correct respiration artifacts, frequency-selective spectral fitting, and quantification using water as an internal reference peak. We quantified 500 in vivo spectra with this technique, analyzed the results, and compared them with an independent method based on external referencing. The applicability of using quantitative ^{1}H MRS for diagnosing suspect breast lesions is discussed below.

MATERIALS AND METHODS

Acquisition

All measurements were performed with a hybrid 4 T system, consisting of a 90-cm-bore magnet (model 4 T-900; Oxford Magnet Technology, Oxfordshire, UK) with a clinical gradient system (Sonata; Siemens, Erlangen, Germany) interfaced with an imaging spectrometer (Unity Inova; Varian, Palo Alto, CA). Several different single-breast quadrature transmit/receive RF surface coils of similar design were used to accommodate different breast sizes. The coils were mounted on a custom-built patient table designed for unilateral, prone breast studies.

A total of 105 subjects (23–72 years old, mean = 48 years) were studied in 175 MRI/MRS sessions. Of these, 86 were participants in a study involving the diagnosis of lesions with suspicious mammographic findings, 14 were participants in a study regarding monitoring response to neoadjuvant chemotherapy, and five were presumed normal volunteers (no breast-related health problems or abnormal mammograms). Approximately half of these studies were performed after a needle biopsy or other invasive procedure. All studies were approved by the institutional review board, and informed written consent was obtained from the subjects prior to the studies.

All 100 patients from the diagnosis and treatment-monitoring studies were examined with the same MRI/MRS protocol, which consisted of high-resolution imaging, dynamic contrast-enhanced imaging, and single-voxel spectroscopy. The subjects were positioned prone with their breast centered horizontally in the magnet. After scout images were acquired to verify position, the coil was manually tuned and matched. A high-resolution 3D fast low-angle shot (FLASH) image (fat-suppressed, matrix = 256 × 256 × 64, field of view (FOV) = 14–18 cm, TE/TR = 4.1/13.5 ms, flip angle = 30°) and a fast 2D multislice image (fat-suppressed, matrix = 256 × 128, 30 slices, slice thickness = 2.5 mm, FOV = 14–18 cm, TE/TR = 5.1/390 ms, flip angle = 90°) were acquired prior to injection of Gd-DTPA (0.1 mmol/kg body weight). Five to seven 2D images were acquired immediately after injection, followed by a second 3D image. Both image sets were analyzed using own image-processing software (developed with Matlab (The Mathworks, Natick, MA)) to select voxels for MRS with the subject still in the magnet. The criteria for voxel selection included lesion architecture, dynamic Gd-DTPA uptake, and prior clinical information from mammographic or ultrasound images. The voxels were planned to maximize coverage of the lesion and minimize the inclusion of adipose tissue. The five normal subjects were studied with only the high-resolution 3D FLASH image followed by spectroscopy, since no Gd-DTPA was administered in these studies.

All spectra were acquired using the LASER localization technique (15) with 4096 complex points and 6-kHz spectral width. Each voxel measurement began with a calibration of the localized B_1 field strength, followed by 30–60 s of manual adjustment of the linear shims. A fully relaxed, single-shot, unsuppressed spectrum was acquired to measure the water and lipid peaks. The power required to suppress the water signal using variable pulse power and optimized relaxation delays (VAPOR) (17) water suppression was then manually adjusted. The metabolite spectrum was acquired using TE averaging with TE = 45–196 ms in 64 or 128 increments and with TR = 3 s (16). Each free induction decay (FID) signal was individually saved, and no averaging was performed until processing. Each voxel required ~9 min in total. One to four voxels were studied in each subject, for a total acquisition time of ~1 hr.

Preprocessing Spectra

All spectral processing programs, including preprocessing, fitting, and quantification, were written in Matlab (The Mathworks, Natick, MA). In all spectra, the last 512 points of the raw TD FID were used to calculate the root-mean-square (RMS) noise and correct for DC offsets. For the unsuppressed spectra used to measure the water and lipid peaks, the FIDs were truncated to 1024 points and then zero-filled to 2048 points. The zero-order phase ϕ was measured and corrected using the average of two different autophasing methods: 1) fitting the phase of the first few TD points to a line and using ϕ at time $t = 0$, and 2) finding the value of ϕ that maximizes the smallest value of the real part of the FD spectrum. Using the mean of these two methods produces a robust estimate of ϕ. The spectra were then frequency referenced by setting the maximum of the water peak to 4.7 ppm. For the water-suppressed spectra used to measure the metabolites, each individual spectrum from the TE averaging acquisition was automatically phased as described above. To correct respiration-induced frequency shifts, each spectrum was shifted in frequency to maximize the cross-correlation function between it and the first spectrum of the acquisition (18). After phasing and frequency correction was performed, the spectra were averaged.

Fitting

To fit the water, 1.3 ppm lipid, and tCho peaks in the processed spectra, a new fitting program was developed.

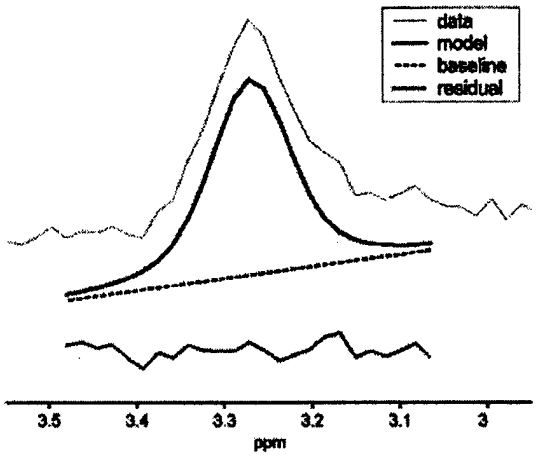

FIG. 1. Model showing the frequency-selective fit of a tCho peak with baseline correction. The real component of the raw data is fit with a Voigt lineshape model (thick line) plus a linear baseline (dashed line). The residual (dotted line) is minimized over a 0.4-ppm region centered around the peak. The same model without the linear baseline is used to fit the unsuppressed water and lipid peaks.

The algorithm is based on the TDFD fitting technique proposed by Slotboom et al. (14). In this approach, a TD model is used to describe the peak parameters, but the fitting is performed by applying a Fourier transform and minimizing the residuals in the FD. This flexible fitting method has excellent frequency-selective properties and can be used with various lineshape definitions. In this implementation, a Voigt lineshape was used to model all peaks (19). The modeled signal s_{model} from a single peak s can be described in the TD t as

$$s_{model}(t) = A \cdot \exp(-i\omega t + i\phi - \lambda t - \gamma^2 t^2) \quad [1]$$

with signal amplitude A, chemical shift frequency ω, zero-order phase ϕ, Lorentzian damping factor λ, and Gaussian damping factor γ. The Lorentzian and Gaussian damping factors are related to the full width at half maximum (FWHM) of an impulse response: $\lambda = \pi \cdot FWHM$ and $\gamma = \pi \cdot FWHM/(2\sqrt{\ln 2})$, as described by Ogg et al. (20). Note that although all equations in this section are shown with continuous time and frequency for clarity, all calculations were performed with discrete variables.

The peaks were fit one at a time by minimizing the FD residuals over a 0.4-ppm (68-Hz) section of the spectrum centered on the peak. The zero-order phase ϕ was fixed at zero (since it was presumably corrected during preprocessing) and only the real portion of the residual was minimized. Initial values for parameters were generated based on prior knowledge and simple heuristics (e.g., the initial frequency is that of the maximum of the absolute value spectrum over the fitting region). The nonlinear minimization of the residuals was performed using the optimization toolkit provided with Matlab (function *lsqnonlin*, using the large-scale model option).

In the unsuppressed spectra, water was fit at 4.7 ppm, and the polymethylene lipid peak was fit at 1.3 ppm. In the suppressed and averaged spectra, tCho was fit at 3.25 ppm. The baseline around 3.25 ppm is often distorted, so a linear baseline model was used to reduce bias. Figure 1 shows the relationship between the data (S_{data}), model (S_{model}), baseline ($S_{baseline}$), and residual (R). Using a linear baseline, the residual function to be minimized is

$$R(\omega) = [S_{data}(\omega) - S_{baseline}(\omega) - FFT\{s_{model}(t)\}]_{\omega_0-0.2ppm}^{\omega_0+0.2ppm} \quad [2]$$

where ω_0 is the center of the frequency range being fit. No baseline correction was used for fitting the water and lipid peaks, so in those cases $S_{baseline} = 0$ for all ω.

The peak amplitude A is the parameter of greatest interest since it is proportional to the number of nuclei in the voxel. The fitting error was estimated using the Cramer-Rao minimum variance bound (CRMVB) of the parameter A:

$$CRMVB_A = \frac{\sigma^2_{noise}}{\int_{\omega_0-0.2ppm}^{\omega_0+0.2ppm} \frac{\partial}{\partial A}[FFT\{s_{model}(t)\}]\, d\omega} \quad [3]$$

where σ^2_{noise} is the variance of white, Gaussian noise. The $CRMVB_A$ is not actually an estimate of the fitting error; rather, it is a theoretical minimum limit for the estimation accuracy. Nevertheless, the $CRMVB_A$ is commonly used in NMR applications to estimate fitting errors (21). Effectively, this measure is the noise variance scaled by the sensitivity of the model to changes in the parameter A. The error is often expressed as a normalized standard deviation (SD): $\sigma_A = \sqrt{CRMVB_A}/A$.

This error estimate was also used to establish the detection criteria. In all cases, a fit was initially performed and the parameter estimates and errors were calculated. If the fitting error for A was greater than a specified threshold, then the fit was rejected and the resonance was considered undetectable. For all of the spectra reported in this paper, the threshold for the normalized error was unity: if $\sigma_A > 1$, the peak was considered undetectable. Although this threshold is statistically arbitrary, it is convenient and roughly corresponds to a signal-to-noise ratio (SNR) of 2–3.

Quantification

The spectral fitting produces an amplitude A for each peak, expressed in arbitrary units (au). To standardize this measurement for use in both internal and external referencing schemes, several corrections must be made to account for experimental conditions and the physical properties of each species. The corrected amplitude A' is:

$$A' = \frac{A}{f_{gain} f_{coil} f_{T_1} f_{T_2}} \quad [4]$$

with correction factors

$$f_{gain} = gain/gain_0 \quad [5]$$

$$f_{coil} = B_1/B_{1,0} \quad [6]$$

$$f_{T_1} \approx 1 - \exp(-TR/T_1) \quad [7]$$

$$f_{T_2} = \frac{1}{N}\sum_{j=1}^{N} \exp(-TE_j/T_2), \quad [8]$$

where *gain* is the receiver gain, B_1 is the local amplitude of the excitation radiofrequency field, TR is the pulse repetition time, and TE is the echo time. The receiver correction factor f_{gain} is necessary if the receiver gain is different in the suppressed and unsuppressed acquisitions. The coil receive efficiency factor f_{coil} was calculated by assuming the transmit and receive efficiencies are equal. The reference values $gain_0$ and $B_{1,0}$ are arbitrary, but must be used consistently when comparing values from different acquisitions. The T_1 correction f_{T_1} is approximate, and is valid provided TR >> TE. With a TE-averaged acquisition, the T_2 correction f_{T_2} is a summation over N acquisitions, each with different a TE (16). Because it is impractical to measure relaxation properties in each voxel, constant values were assumed for all relaxation constants based on measurements in several subjects.

After these corrections are made, the signal amplitudes are proportional to the number of nuclei in the volume. The ratio of the tCho and water amplitudes can be converted to molal concentration (moles solute per mass solvent) by correcting for the number of ^1H nuclei per molecule η and the molecular weight of the solvent MW_{water}:

$$[\text{tCho}] = \left(\frac{A}{f_{gain} f_{T_1} f_{T_2}}\right)_{tCho} \left(\frac{f_{gain} f_{T_1} f_{T_2}}{A}\right)_{water} \frac{\eta_{water}}{\eta_{tCho} MW_{water}}. \quad [9]$$

Note that the coil efficiency factor f_{coil} cancels because both water and tCho come from the same volume of interest. This quantity [tCho], expressed in units mmol/kg, is the metric proposed as an in vivo measure of the tissue level of choline-containing compounds in the breast. This measurement is presented along with the SD of the fitting error: [tCho] ± [tCho] · σ_A.

In spectra where no tCho peak was detected based on the $\sigma_A > 1$ criterion, an additional procedure was performed to determine the sensitivity of the measurement. A simulated, noiseless spectrum containing a single peak at 3.25 ppm with a Gaussian FWHM of 15 Hz and amplitude A_{sim} was added to the preprocessed in vivo spectrum. The combined in vivo + simulated spectrum was then fit using the procedure described above, and the fitting error σ_A was calculated. This process was repeated with successively smaller simulated peak amplitudes, reduced 10% each iteration, until the simulated peak was no longer detectable. The smallest value of A_{sim} that led to a detectable tCho peak was then used to calculate a minimum detectable level (MDL) of tCho, $[\text{tCho}]_{MDL}$, using Eq. [9]. For these in vivo spectra where tCho is not detectable, the overall [tCho] measurement is expressed as 0 ± $[\text{tCho}]_{MDL}$.

To validate this proposed internal referencing scheme, the tCho level was also calculated independently using an external referencing scheme. In general, the corrected signal amplitude A' of a resonance is proportional to the number of nuclei n in the sample: $n = \kappa_{sys} A'$. The system constant κ_{sys} (with units mol/au) accounts for the system-specific hardware and software. The value of κ_{sys} was calculated for our system in separate calibration experiments with a phantom of known concentration and measurable relaxation properties. The externally-referenced concentration of tCho can then be expressed in molal units (mol/kg) as

$$[\text{tCho}]_{ext} = \left(\frac{A}{f_{gain} f_B f_{T_1} f_{T_2}}\right)_{tCho} \frac{\kappa_{sys}}{\eta_{tCho}} \frac{1}{V\rho_{water}} \quad [10]$$

where ρ_{water} is the water density, and V is the voxel volume. To compare the internal and external methods, the tissue water density was assumed to be 1 kg/L. The volume V was assumed to be the entire voxel volume, ignoring the effect of partial volume from adipose tissue.

RESULTS

The quantification method was applied to 500 spectra acquired from 105 subjects in 175 MR study sessions. The voxel size ranged from 0.4 to 16 mL, with a median volume of 1.6 mL. A peak near 3.25 ppm was detected in 214 (43%) of the 500 spectra. The processing and fitting processes required ~1 min per spectrum on a typical workstation. After we ran the fully-automated procedure on all 500 spectra and manually reviewed the results, six spectra required reprocessing with manual intervention to adjust phase and/or frequency referencing. Each water, lipid, and tCho peak was fit with a Voigt lineshape, giving both Lorentzian and Gaussian contributions to the linewidth. The fit water peak had a median Lorentzian and Gaussian linewidth of 12 Hz and 13 Hz, respectively; the 1.3 ppm lipid peak had 16 Hz and 28 Hz, and the tCho peak had 0 Hz and 14 Hz.

To calculate absolute tCho levels, relaxation values were measured in several subjects using standard spectroscopic techniques. The measured values with SDs were: $T_{1,water}$ = 870 ± 325 ms, $T_{2,water}$ = 60 ± 7 ms, $T_{1,lipid}$ = 480 ± 100 ms, $T_{2,lipid}$ = 69 ± 12 ms, and $T_{2,tCho}$ = 399 ± 133 ms. $T_{1,tCho}$ was not measured, but was assumed to be the same as $T_{1,water}$. Although some of these SDs are large, their overall effect on the [tCho] measurement is relatively small. Using our acquisition parameters, the uncertainties in $T_{1,water}$, $T_{2,water}$, $T_{1,tCho}$, and $T_{2,tCho}$ led to [tCho] SDs of 0%, 5%, 6%, and 13%, respectively, for a total of 16%.

Several examples of in vivo spectra are shown in Fig. 2. Figure 2a shows a large voxel acquired in healthy glandular tissue. A clear tCho peak is visible at 3.25 ppm, and the fitting produces a measurement of [tCho] = 0.66 ± 0.06 mmol/kg. The model fit of this peak is shown above the full spectrum, and the smooth residual is shown beneath. There is another metabolite peak visible at 3.4 ppm that was not fit. This sample shows that tCho can be detected in normal breast tissue. Figure 2b is a spectrum from an invasive ductal carcinoma with [tCho] = 6.1 ± 0.08 mmol/kg. The volume of this voxel is smaller than that of the voxel in Fig. 2a, but since it is located closer to the coil the sensitivity is comparable. The SNR of the tCho peak is quite high, but the residual shows some structure, indicating an imperfect fit. Figure 2c shows a more typi-

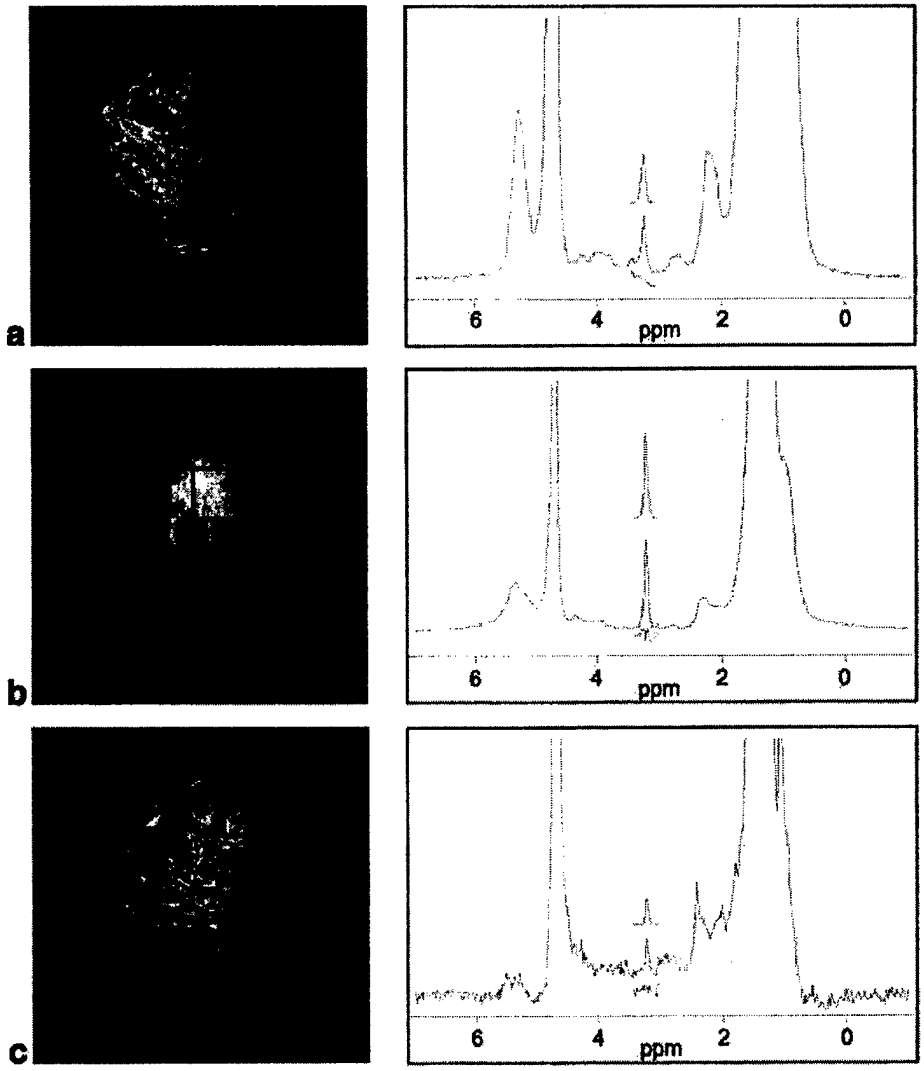

FIG. 2. Example spectra. A water-suppressed spectrum is shown on the right, with the tCho fit shown above and the residual (including linear baseline) underneath. The location of the voxel is shown in a contrast-enhanced, fat-suppressed sagittal image on the left. **a:** Normal gland, volume = 13.0 mL, [tCho] = 0.66 ± 0.06 mmol/kg, lipid fraction = 3%. **b:** Malignant tumor of invasive ductal carcinoma, volume = 6.8 mL, [tCho] = 6.1 ± 0.08 mmol/kg, lipid fraction = 8%. **c:** Benign finding of atypical hyperplasia in an insensitive region of the coil, volume = 1.1 mL, [tCho] = 1.4 ± 0.7 mmol/kg, lipid fraction = 14%.

cally-sized voxel in a lesion later identified by needle biopsy as atypical hyperplasia, with [tCho] = 1.5 ± 0.8 mmol/kg. Atypical hyperplasia is generally considered to be benign, but it is a marker indicating an increased risk for developing future malignancies. The low SNR of the tCho peak is reflected in the error estimated by the fitting procedure.

These examples demonstrate how the sensitivity of breast MRS can vary greatly. Due to variability in coil loading, voxel size, and partial volume of adipose tissue, the sensitivity for detecting tCho varied by a factor of >100 in this study. Figure 3 shows the fitting error in all 500 spectra as a function of water SNR and voxel volume. For both natural and simulated spectra, the fitting error is the normalized error multiplied by the calculated concentration, $[tCho] \cdot \sigma_A$ or $[tCho]_{MDL} \cdot \sigma_A$. Clearly, the water SNR is a better indicator of fitting error, since it automatically corrects for coil efficiency and the partial volume of adipose tissue. These plots show reasonable properties for an unbiased fitting method. For example, fitting error decreases uniformly with increasing water SNR, and tCho is more likely to be detected in spectra with lower fitting errors.

Although the fitting error is greater in smaller voxels, the [tCho] measurement itself is independent of the voxel size, as shown in Fig. 4a. The filled diamonds represent [tCho]

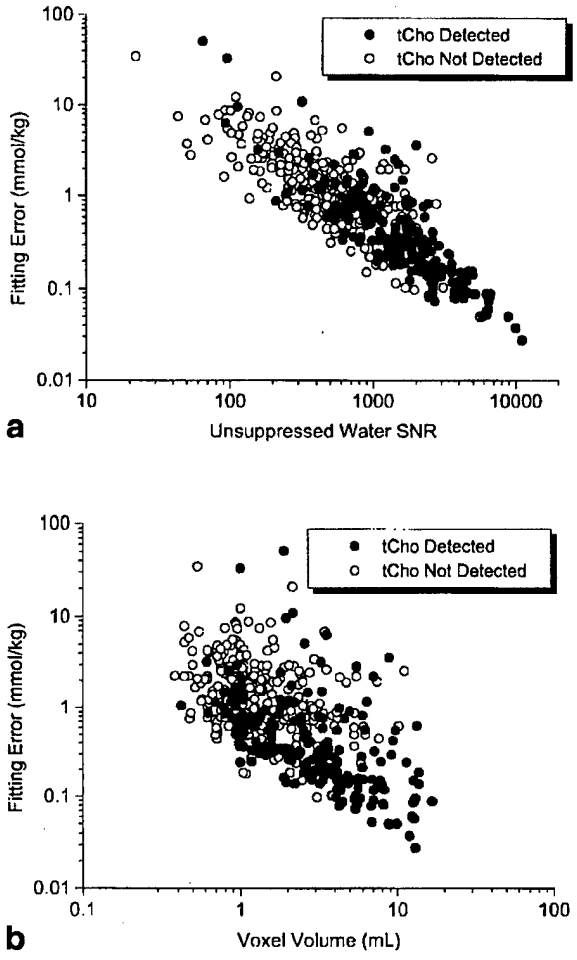

FIG. 3. Factors contributing to the sensitivity of [tCho] measurement. **a:** The fitting error from all 500 spectra as a function of the SNR of the unsuppressed water peak (TD amplitude/RMS noise). **b:** The fitting error as a function of total voxel volume. Filled circles are error estimates from spectra where tCho was detectable; open circles are error estimates calculated using the MDL procedure (see text) from spectra where no tCho was detectable.

measurements in spectra where a peak was detectable, and the hollow diamonds represent the MDL of tCho in spectra where no peak was detectable. As expected, the smaller voxels were less likely to have detectable tCho, but clearly the voxel size did not bias the [tCho] measurement in spectra with detectable tCho.

Figure 4b shows how the [tCho] measurement varies with the lipid content of the voxel. The lipid fraction is estimated using the ratio between the corrected amplitudes of the water and 1.3 ppm lipid peaks: % = $A'_{\text{lipid}}/(A'_{\text{water}} + A'_{\text{lipid}}) \times 100$. The [tCho] measurement was expected to be independent of the voxel lipid fraction because all of the metabolites that contribute to the tCho peak are water-soluble. In voxels with low to moderate lipid content, [tCho] was independent of the lipid fraction. In voxels with large lipid content, however, the [tCho] measurement increases with increasing lipid fraction. Lipids apparently contribute to the amplitude of the tCho peak, either through baseline artifacts not suppressed by TE averaging or by a true resonance at 3.25 ppm. Because of this lipid contamination, we arbitrarily chose a cutoff value of 33%, above which the [tCho] measurement is considered biased and the MRS measurement is considered invalid.

Figure 5 shows a comparison between the internal and external reference schemes described in Materials and Methods. This shows that in good-quality spectra, where tCho is detectable and the lipid content is low, both internal and external methods produce consistent results (R^2 = 0.91). The absolute values produced by the external method are lower, due to overestimation of the product ($V \cdot$

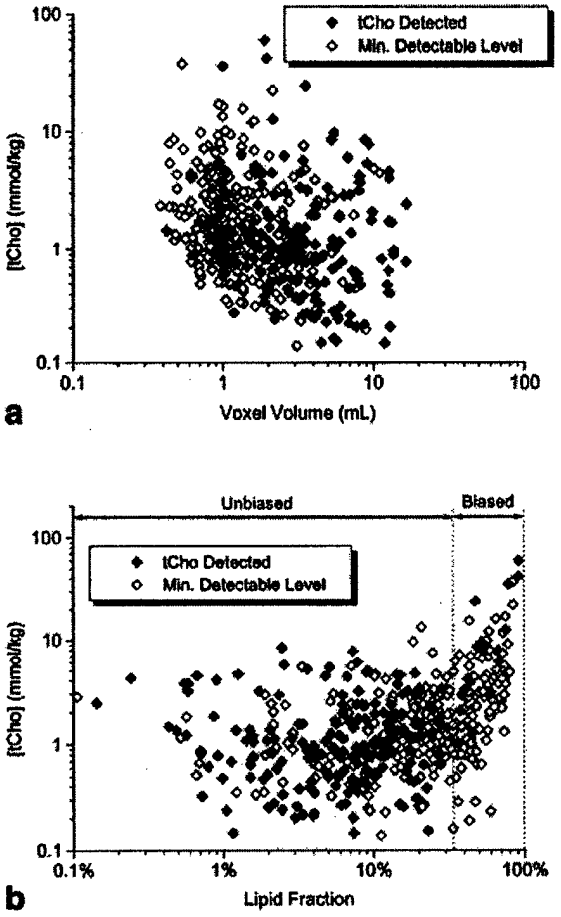

FIG. 4. Dependence of [tCho] on voxel volume and lipid content. The [tCho] measurements from spectra where tCho was detectable are indicated by solid diamonds; for spectra where tCho did not meet the detectability threshold, the MDLs of tCho are indicated by hollow diamonds. Part **a** shows that the [tCho] measurement is independent of voxel volume, which is desirable. Part **b** shows that when the lipid volume fraction is low, the [tCho] measurement is unbiased. When the lipid content is high, the [tCho] measurement increases. Spectra with lipid fractions > 33% (an arbitrarily selected threshold) are considered biased.

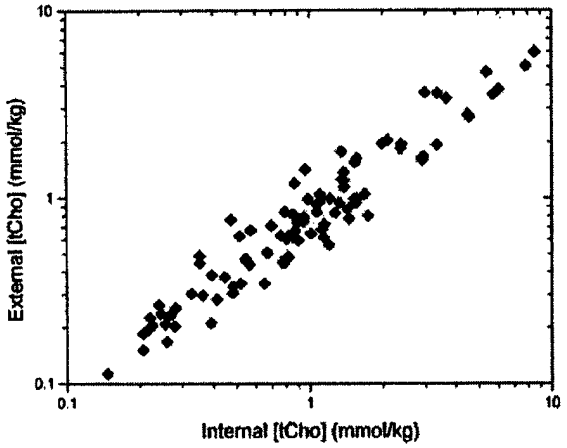

FIG. 5. A comparison between [tCho] calculated with both internal and external referencing methods in 98 spectra, all of which had detectable tCho and a lipid fraction of ≤33%. A linear fit through the origin gives $R^2 = 0.91$ and a slope of 0.72. This shows that these measures are highly correlated, although the external method produces somewhat smaller values.

ρ_{water}) in the denominator of Eq. [10], which represents the aqueous content of the voxel.

The applicability of the [tCho] measurement for diagnosing different pathologies is shown in Fig. 6. All spectra that were of sufficient quality (i.e., free of artifacts, lipid fraction ≤ 33%) and were acquired from lesions with biopsy-confirmed pathology were divided into a "malignant" category (including infiltrative ductal, lobular, and unspecified carcinomas) and a "benign" category (including atypical hyperplasias, fibroadenomas, fibrocystic changes, and cysts). There were insufficient data to distinguish further histological subcategories or tumor-staging grades. When multiple spectra were acquired from a single lesion, only the spectrum with the smallest error was included in this chart. Spectra labeled "normal" were acquired from normal volunteers and from regions of normal-appearing and asymptomatic glandular tissue in other subjects. These results show that the tCho measurement is elevated in malignancies and some benign lesions. The mean [tCho] is greater in malignancy than in benign tissues ($P = 0.008$, one-tailed t-test), but the difference between the normal and benign categories is not statistically significant ($P = 0.17$). An ROC analysis was performed to determine a threshold [tCho] value for distinguishing between benign and malignant lesions. Using equal weighting for false positives and false negatives, the criteria for malignancy is [tCho] ≥ 1.38 mmol/kg. With this cutoff, the sensitivity is 46% and the specificity is 94%. Note that neither of these analyses take into account the variable sensitivity.

Single-voxel MRS in the breast is very sensitive to the size and placement of the voxel because of the heterogeneous distribution of tCho in the breast, as can be seen in the spectra shown in Fig. 7. All three spectra were acquired from different regions of the same 3-cm tumor, a grade III invasive ductal carcinoma that was studied after the patient had received 4 months of chemotherapy. In a large voxel covering most of the tumor, [tCho] was measured to be 1.1 ± 0.6 mmol/kg. The anterior, enhancing portion of the tumor had a higher [tCho] (1.5 ± 0.5 mmol/kg), whereas the posterior, non-enhancing region had no detectable peak ([tCho] = 0 ± 1.3 mmol/kg). The sensitivity is lowest in the posterior voxel due to its distance from the coil, small voxel size, and higher lipid content. This example underscores the importance of proper voxel placement.

DISCUSSION

This work describes a new method for quantifying tCho levels in breast tissue. Quantitative MRS is a substantial improvement over the qualitative detection methods used in previous studies of breast MRS. Quantification is particularly important in the breast because the sensitivity of the MRS measurement is generally more variable than it is in brain tissue. This is due primarily to the highly variable adipose tissue content of the breast and the greater variation of the coil receive efficiency. Previous in vivo studies used the hypothesis that detectability of tCho is associated with malignancy; however, this approach is only valid if the detection threshold is constant. We have found that the use of a higher B_0 field (4 T) and optimized surface coils increases the sensitivity enough to enable the detection of tCho in normal breast tissue and several benign lesions.

Two previous reports used external referencing to quantify choline levels in breast tissue (7,13). Neither of these studies corrected for partial volume of adipose tissue within the voxel. In our experience, the amount of intravoxel adipose tissue can vary greatly, as shown in Fig. 4b. The breast can be coarsely approximated by a two-compartment model consisting of aqueous regions (fibroglandular tissue) and aliphatic regions (adipose tissue). The aqueous compartment contains all of the choline-containing compounds that are known to be elevated in malignan-

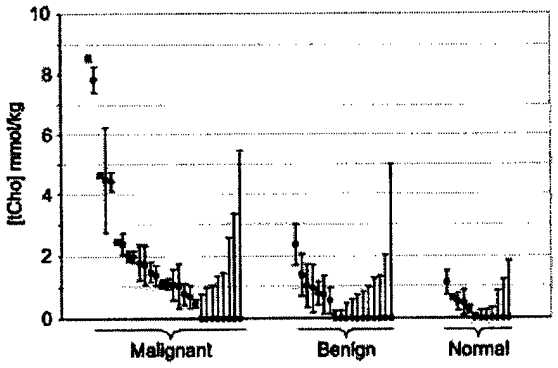

FIG. 6. Measurements of [tCho] in malignant, benign, and normal tissues. Error bars represent SDs in spectra where tCho was detectable, and MDLs in spectra where no tCho was detectable. Measurements are ordered from the largest to the smallest in each category. Malignant and benign spectra were from biopsy-confirmed lesions only. Normal spectra were selected from healthy-appearing glandular tissue.

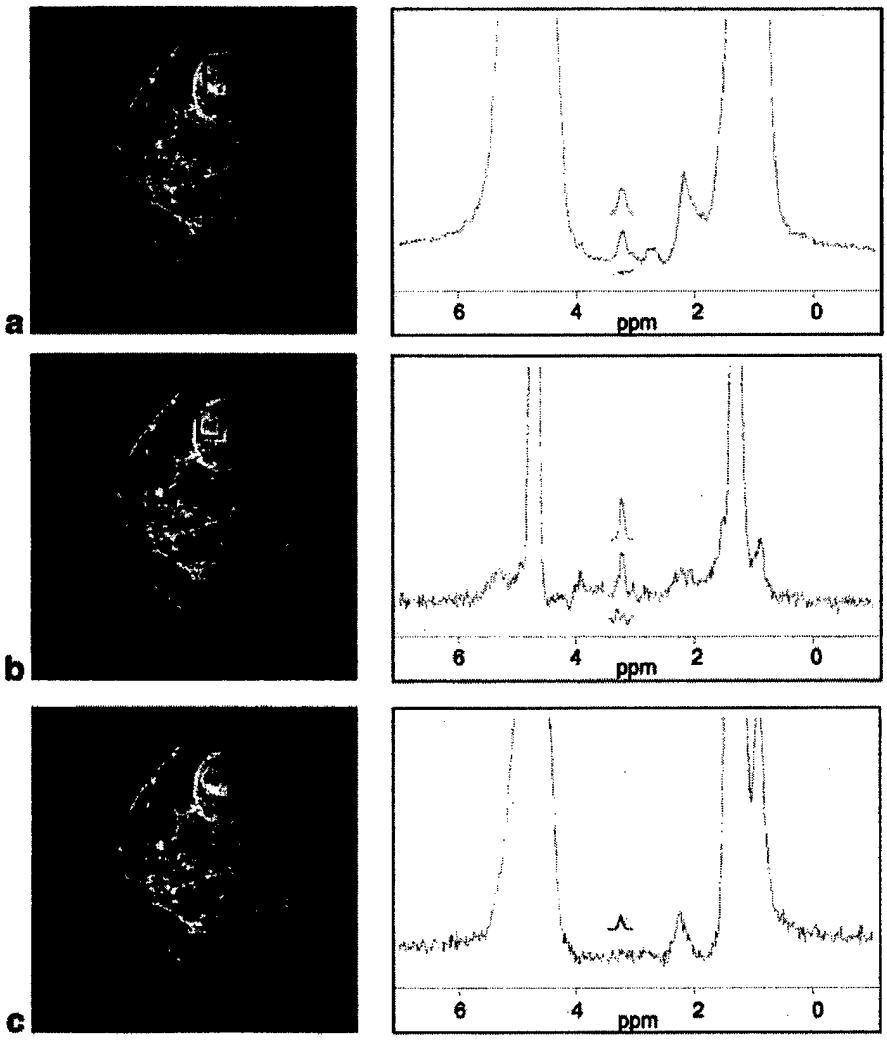

FIG. 7. Spatial variation of [tCho] measurements within a single tumor. All spectra are from a 3-cm tumor of invasive ductal carcinoma after 4 months of chemotherapy treatment. Images on the left show voxel positions on a sagittal slice from a contrast-enhanced, fat-suppressed 3D FLASH image. Water-suppressed spectra on the right are shown with the tCho fit above and the residual (including baseline) underneath. In spectrum C, where no tCho was detectable, the MDL of tCho is shown with a dotted line. **a:** Voxel containing both enhancing and non-enhancing regions of the tumor, volume = 7.8 mL, [tCho] = 1.1 ± 0.6 mmol/kg, lipid fraction = 5%. **b:** Voxel acquired from the most enhancing region of the tumor, volume = 1.1 mL, [tCho] = 1.5 ± 0.5 mmol/kg, lipid fraction = 2%. **c:** Voxel acquired from a non-enhancing region, volume = 0.9 mL, [tCho] = 0 ± 1.3 mmol/kg, lipid fraction = 13%.

cies. Any externally-referenced method must account for this compartmentation to avoid systematic error, whereas an internally-referenced method compensates for compartmentation automatically. Internal referencing methods have further advantages in that they do not require separate calibration experiments, and they use fewer error-introducing correction factors for coil loading, coil efficiency, and voxel volume.

The disadvantage of the internal referencing approach is that it requires the density of NMR-visible water in the aqueous compartment to be relatively constant. There are physiological conditions that affect the water content, but these effects are expected to be small compared to the variability of compartmentation. Both internal and external approaches will be affected by the presence of edema from previous invasive procedures or radiation therapy, and by variations in cellularity and relaxation rates. Previous reports expressed concern that the relaxivity of gadolinium contrast agents would deleteriously affect MRS measurements (8). In our experience, gadolinium effects are small (~10%) compared to the measurement errors and variability of tCho levels (22).

The spectral fitting software used in this work is highly specialized for fitting peaks in breast spectra, and is available from the authors by request. The method is based on the TDFD fitting technique, which uses an analytical TD

model but minimizes residuals in the FD (14). We modified that technique by adding a linear baseline correction and using a very narrow frequency band (0.4 ppm) to fit a single peak at a time. By using only the real component of the spectrum, along with the narrow frequency band and the linear baseline correction, small tCho peaks can be fit without bias from large neighboring lipid resonances. Another useful feature of the TDFD method is that it permits the use of the Voigt lineshape, which can fit purely Lorentzian or purely Gaussian lineshapes, or any combination of the two. This flexibility was useful for this application because the use of a Lorentzian or Gaussian model alone did not produce good-quality fits for all peaks. The tCho peak is difficult to model precisely because it is a superposition of several resonances, and at 4 T there is not sufficient spectral resolution to separate the individual components. Also, imperfect correction of respiration-induced frequency shifts can cause "blurring" that leads to Gaussian lineshapes in averaged spectra. Although the Voigt model did not always produce an ideal fit (e.g., Fig. 2b), it performed reasonably well in most cases.

The TDFD method was chosen because it is well suited to the problem and is relatively easy to implement. There are numerous other methods that could be adapted for fitting breast spectra; however, most of these methods are incapable of fitting a precise frequency range or analytically modeling a non-Lorentzian lineshape (23,24). The LCModel method (25) is very useful for fitting brain spectra, and it may also be applicable for fitting breast spectra. With the currently available implementation of the LCModel software, we were unable to get good-quality fits of small tCho peaks in spectra with large lipids. If the LCModel method could be adapted for breast spectra, it might offer some advantages, such as producing more accurate fits due to its sophisticated baseline model, and enabling the fitting of other metabolites that are occasionally observable in breast spectra, such as creatine, glycine, lactose, and taurine. Automated fitting methods are generally desirable because they eliminate user interaction and provide a well accepted measure of error (Cramer-Rao bounds) unbiased by peak lineshape. However, a simple analysis using peak integration and linear baseline correction over manually-defined extents gave comparable results (data not shown).

Investigators commonly use CRMVBs to estimate the variance of model parameters when fitting NMR spectra (21). In this work, the fitting error is used as an estimate of the overall measurement error, although it is possibly an underestimate. Most notably, the CRMVB errors from fitting the water are very small, but the actual error in estimating the water amplitude is higher. This occurs because the Cramer-Rao theory assumes that the data are perfectly described by the model function, and this assumption is violated by irregular water lineshapes and the overlapping 5.4 ppm lipid resonance. Additionally, certain experimental factors (e.g., patient motion and respiration) can make the true measurement error greater than the fitting error. The true measurement error can only be established through repeatability studies. Nevertheless, some estimate of the measurement error is essential for any quantification scheme, and it should be incorporated into the interpretation of quantitative MRS results. It is particularly important in breast MRS because of its highly variable sensitivity, as demonstrated in Fig. 3a. Note that this sensitivity can be estimated prior to the acquisition of an entire spectrum by using the SNR of the water peak in a single-shot, unsuppressed spectrum. This information can be used to prescreen voxels for a diagnostic study.

The iterative MDL method described here (in which a simulated tCho peak is added to a spectrum and fit) can be used to measure the sensitivity in spectra with no detectable tCho peak. This is critical for interpreting whether a negative finding of tCho is due to lack of sensitivity or low tCho levels. The MDL is closely related to the fitting error: under ideal conditions, the fitting error is equal to the MDL, but in practice the MDL is often larger.

The use of a quantitative method to measure tCho levels in the breast increases the usefulness of MRS for diagnosing benign and malignant lesions. Figure 6 shows [tCho] measurements divided into three broad pathological categories. The finding that tCho levels are higher in malignancies than in benign or normal tissues is consistent with previously published reports that used the detection of tCho to indicate malignancy (7–11). The [tCho] threshold of 1.38 mmol/kg, based on an ROC analysis, can be used to distinguish between malignant and benign lesions; however, the sensitivity is poor (46%). More data must be acquired to determine whether subdividing the malignant and benign categories will improve these results (e.g., in the benign category, the two highest values were atypical hyperplasias). Note also that this ROC analysis is only a first-order method of interpreting the [tCho] levels. More sophisticated analyses should be used to account for the measurement errors and [tCho] probability distribution functions.

The absolute tCho levels (0.4–10 mmol/kg) reported in this work are reasonably consistent with previous in vivo estimates. Roebuck et al. (7) found choline levels of 0.4–5.8 mmol/L, and estimated their detection threshold was 0.2 mmol/L. Bakken et al. (13) reported a single measurement of 2 mmol/L. Further investigations are required to determine whether the absolute [tCho] values reported here are reproducible on different MR scanners and in other institutions.

Figure 6 shows a large range of [tCho] measurements in known cancers, from 0.5 to >8 mmol/kg. tCho levels did not appear to be related to different histological types of cancer (e.g., lobular vs. ductal); however, there were insufficient data to establish statistical significance. The variation in [tCho] was also not explained by complicating factors such as recent biopsy or previous chemotherapy treatments, although some of the spectra in which no tCho was detected were acquired from tumors that had been recently biopsied. The large range in [tCho] measurements may be a natural feature of cancer, due to variations in the amount of water, lipids, and stroma within the lesion and adjacent tissues, and to variations in intracellular tCho levels and neoplastic cell density. Previous chemotherapy, radiation, or invasive procedures may further complicate these issues. Additionally, certain experimental factors can contribute to inaccuracy in these measurements—most notably patient motion and incorrect voxel positioning. If either the biopsy needle or the MRS voxel is placed in the

wrong region, there will be no agreement between the [tCho] measurements and the histology. Finally, it should be noted that MRS measurements can be adversely affected by metallic radiographic markers, which are widely used but cannot always be identified in heterogeneous breast tissue.

CONCLUSIONS

In this work we report a new technique for quantifying tCho levels in breast cancer using single-voxel ^{1}H MRS. With the use of optimized surface coils and a high-field (4 Tesla) scanner, we measured tCho levels in normal breast tissue and in benign and malignant lesions. The levels of tCho were found to be elevated in malignancies compared to benign lesions, indicating that quantitative MRS may be used to aid in diagnosing breast lesions and monitoring response to cancer treatments.

ACKNOWLEDGMENTS

We thank Bibi Husain, Lou Forsythe, R.N., and Julie Gay, R.N., for recruiting and scheduling the research subjects; and Robin Bliss, M.S., and Chap Le, Ph.D., for consultations on biostatistics.

REFERENCES

1. Kopans DB. Breast imaging, 2nd ed. Philadelphia: Lippincott-Raven; 1998. 875 p.
2. Howe HL, Wingo PA, Thun MJ, Ries LA, Rosenberg HM, Feigal EG, Edwards BK. Annual report to the nation on the status of cancer (1973 through 1998), featuring cancers with recent increasing trends. J Natl Cancer Inst 2001;93:824–842.
3. Orel SG, Schnall MD. MR imaging of the breast for the detection, diagnosis, and staging of breast cancer. Radiology 2001;220:13–30.
4. Mackinnon WB, Barry PA, Malycha PL, Gillett DJ, Russell P, Lean CL, Doran ST, Barraclough BH, Bilous M, Mountford CE. Fine-needle biopsy specimens of benign breast lesions distinguished from invasive cancer ex vivo with proton MR spectroscopy. Radiology 1997;204:661–666.
5. Gribbestad IS, Sitter B, Lundgren S, Krane J, Axelson D. Metabolite composition in breast tumors examined by proton nuclear magnetic resonance spectroscopy. Anticancer Res 1999;19:1737–1746.
6. Aboagye EO, Bhujwalla ZM. Malignant transformation alters membrane choline phospholipid metabolism of human mammary epithelial cells. Cancer Res 1999;59:80–84.
7. Roebuck JR, Cecil KM, Schnall MD, Lenkinski RE. Human breast lesions: characterization with proton MR spectroscopy. Radiology 1998;209:269–275.
8. Kvistad KA, Bakken IJ, Gribbestad IS, Ehrnholm B, Lundgren S, Fjosne HE, Haraldseth O. Characterization of neoplastic and normal human breast tissues with in vivo 1H MR spectroscopy. J Magn Reson Imaging 1999;10:159–164.
9. Yeung DK, Cheung HS, Tse GM. Human breast lesions: characterization with contrast-enhanced in vivo proton MR spectroscopy—initial results. Radiology 2001;220:40–46.
10. Cecil KM, Schnall MD, Siegelman ES, Lenkinski RE. The evaluation of human breast lesions with magnetic resonance imaging and proton magnetic resonance spectroscopy. Breast Cancer Res Treat 2001;68:45–54.
11. Jagannathan NR, Kumar M, Seenu V, Coshic O, Dwivedi SN, Julka PK, Srivastava A, Rath GK. Evaluation of total choline from in-vivo volume localized proton MR spectroscopy and its response to neoadjuvant chemotherapy in locally advanced breast cancer. Br J Cancer 2001;84:1016–1022.
12. Katz-Brull R, Lavin PT, Lenkinski RE. Clinical utility of proton magnetic resonance spectroscopy in characterizing breast lesions. J Natl Cancer Inst 2002;94:1197–1203.
13. Bakken IJ, Gribbestad IS, Singstad TE, Kvistad KA. External standard method for the in vivo quantification of choline-containing compounds in breast tumors by proton MR spectroscopy at 1.5 Tesla. Magn Reson Med 2001;46:189–192.
14. Slotboom J, Boesch C, Kreis R. Versatile frequency domain fitting using time domain models and prior knowledge. Magn Reson Med 1998;39:899–911.
15. Garwood M, DelaBarre L. The return of the frequency sweep: designing adiabatic pulses for contemporary NMR. J Magn Reson 2001;153:155–177.
16. Bolan PJ, DelaBarre L, Baker EH, Merkle H, Everson LI, Yee D, Garwood M. Eliminating spurious sidebands in 1-H MRS of breast lesions. Magn Reson Med 2002;48:215–222.
17. Tkac I, Starcuk Z, Choi IY, Gruetter R. In vivo 1H NMR spectroscopy of rat brain at 1 msec echo time. Magn Reson Med 1999;41:649–656.
18. Henry P-G, van de Moortele P-F, Giacomini E, Nauerth A, Bloch G. Field-frequency locked in vivo proton MRS on a whole-body spectrometer. Magn Reson Med 1999;42:636–642.
19. Marshall I, Higinbotham J, Bruce S, Freise A. Use of Voigt lineshape for quantification of in vivo 1H spectra. Magn Reson Med 1997;37:651–657.
20. Ogg RJ, Kingsley PB, Taylor JS. The line broadening and unambiguous specification of the Gaussian filter. J Magn Reson A 1995;117:113–114.
21. Cavassila S, Deval S, Huegen C, van Ormondt D, Graveron-Demilly D. Cramer-Rao bounds: an evaluation tool for quantitation. NMR Biomed 2001;14:278–283.
22. Bolan PJ, Baker E, DelaBarre L, Merkle H, Yee D, Everson LI, Garwood M. Effects of Gd-DTPA on breast 1H MRS at 4T. In: Proceedings of the 87th Annual Meeting of RSNA, Chicago, 2001.
23. Vanhamme L, Sundin T, Hecke PV, Huffel SV. MR spectroscopy quantitation: a review of time-domain methods. NMR Biomed 2001;14:233–246.
24. Mierisova S, Ala-Korpela M. MR spectroscopy quantitation: a review of frequency domain methods. NMR Biomed 2001;14:247–259.
25. Provencher SW. Estimation of metabolite concentrations from localized in vivo proton NMR spectra. Magn Reson Med 1993;30:672–679.

PREDICTING RESPONSE TO NEOADJUVANT CHEMOTHERAPY OF LOCALLY ADVANCED BREAST CANCER WITH *IN VIVO* ^{1}H MRS: A PILOT STUDY AT 4 TESLA

Sina Meisamy, M.D.[1,2], Patrick J. Bolan, Ph.D. [1,2], Eva H. Baker, M.D., Ph.D. [1,2], Robin L. Bliss, M.S.[3], Evin Gulbahce, M.D.[4], Lenore I. Everson, M.D.[2], Michael T. Nelson, M.D. [2], Timothy Emory, M.D. [2], Todd M. Tuttle, M.D. [5], Douglas Yee, M.D. [3,6], Michael Garwood, Ph.D. [1,2,3,*]

[1]The Center for Magnetic Resonance Research, [2]Department of Radiology, [3]Cancer Center, [4]Department of Pathology/Laboratory Medicine, [5]Department of Surgery, [6]Department of Medicine, University of Minnesota School of Medicine, Minneapolis, Minnesota, USA

[*]Send Correspondence to:

Michael Garwood, Ph.D.
Center for Magnetic Resonance Research
2021 Sixth Street SE
Minneapolis, MN 55455
Email: gar@cmrr.umn.edu
Phone: 612-626-2001
Fax: 612-626-2004

Please note that this work has been originated from the same address as the address of the corresponding author.

This original research was presented in part at the 2003 RSNA meeting December 2, 2003 (for which the first author received the Research Trainee Prize). Abstract #750

Grants:

- DOD Breast Cancer Research Program DAMD 17-01-1-0331
- NIH grants RR08079, CA92004, RR00400
- Tickle Family Land Grant Endowment in Breast Cancer Research
- PHS Cancer Center Support Grant P30 CA77398
- Lillian Quist-Joyce Henline Chair in Biomedical Research

Abstract

Purpose: To determine if changes in the concentration of choline-containing compounds ([tCho]) from before to within 24 hours after receiving primary systemic therapy (PST) predict clinical response in patients with locally advanced breast cancer (LABC).

Materials and Methods: Sixteen women with biopsy-confirmed LABC scheduled for doxorubicin-based PST were recruited. Four Tesla MRI/MRS scans were performed prior to treatment, within 24 hours after the first dose, and after the fourth dose of PST. Lesions size was assessed with Gd—DTPA enhanced MRI. Lesion [tCho] was quantified using single-voxel proton (^{1}H) MRS. Statistical analyses used Pearson's correlation coefficient and Wilcoxon rank-sum test.

Results: Fourteen of 16 patients completed the protocol. [tCho] was not measurable in one patient due to unfavorable lesion morphology for MRS voxel placement. Of the remaining 13 patients, 4 had inflammatory breast cancer, 6 had invasive ductal carcinoma (IDC), 2 had invasive lobular carcinoma (ILC), and 1 had mixed IDC/ILC. Based on RECIST criteria, 8/13 patients were objective responders and 5/13 were nonresponders. The change in [tCho] between baseline and within 24 hours after the first dose of PST showed significant positive correlation with the change in lesion size ($R = 0.79$, $p = 0.001$). The change in [tCho] within 24 hours was significantly different between objective responders and nonresponders ($p = 0.007$).

Conclusion: These results suggest that the change in [tCho] between the baseline scan and within 24 hours after the first dose of PST can serve as an indicator for predicting clinical response to doxorubicin-based chemotherapy in LABC.

Introduction

Primary systemic therapy (PST), also known as neoadjuvant chemotherapy, given prior to breast cancer surgery offers several advantages over standard post-operative chemotherapy. Although PST does not offer any survival benefits over post-operative chemotherapy (1, 2), patients who receive PST are more likely to receive breast-conserving surgery. Moreover, the use of PST permits *in vivo* monitoring of tumor response. Complete disappearance of tumor at surgical resection (pathologic complete response) was associated with the best overall survival in multiple studies (2-4). Since there are many active agents to treat breast cancer, it is important to know early in the course of treatment whether the drug chosen will be effective for an individual.

Currently there are no standardized criteria that can individually detect early response to PST. Conventional modalities such as physical examination, ultrasonography, and mammography vary in reliability for measuring tumor response (5-8). MRI is increasingly being used to evaluate locally advanced breast cancer (LABC) defined as invasive carcinomas ≥ 2 cm in longest diameter with or without inflammatory features. With respect to treatment monitoring, studies have shown correlation between specific MRI findings and clinical response. Changes in lesion size, neoplastic phenotype, dynamic contrast enhancement, and extraction flow product all correlate with clinical response (9-15). However, changes in lesion size or dynamic contrast enhancement measured by MRI are not detected until at least 6 weeks following PST (13). The ability to immediately detect response to a specific chemotherapeutic regimen would be ideal, since it would allow for optimal individualization of chemotherapeutic regimens for patients with the goal of obtaining a pathologic complete response.

Recently there has been an interest in the use of proton magnetic resonance spectroscopy (^{1}H MRS) for detecting and monitoring patients with breast cancer. Using ^{1}H MRS, it has been shown that neoplastic breast tissue contains elevated levels of choline-containing compounds (tCho) which yield a signal at a chemical shift of 3.2 ppm (16-20). One group of researchers has shown that changes in the tCho signal occur in breast cancer patients who receive PST (21). Other studies have shown a correlation between the change in tCho signal and clinical response in patients with extracranial lymphomas and germ cell tumors (22) and pediatric gliomas (23).

^{1}H MRS of the breast is technically challenging because sensitivity can be limiting and spectral artifacts can occur. Due to the heterogeneous distribution of fat and glandular tissue in the breast, ^{1}H spectra of breast often contain large lipid signals that give rise to contaminant peaks around 3.2 ppm. Fortunately, these artifactual peaks, also known as sidebands, can be suppressed using a recently developed technique called echo-time (TE) averaging (24). Additionally, treatment monitoring requires implementation of a method to quantify spectra. Previous studies at lower magnetic field strength (1.5 T) were based on the hypothesis that tCho is detectable only in malignant breast tissue (20). However, with the increased sensitivity at high field (4T), it has been shown that tCho is also detectable in benign lesions and normal fibroglandular breast tissue (25).

We hypothesized that an early decrease in the concentration of choline-containing compounds ([tCho]) could identify an early response to PST. Thus, the purpose of our

study was to determine if changes in [tCho] from before to within 24 hours after PST predict clinical response in patients with LABC.

Materials and Methods

Patients

Women between the ages of 18 — 80 years old with biopsy-confirmed LABC who were scheduled to receive doxorubicin-based PST were eligible to enroll in our prospective study. Patients were enrolled in our study from August 2001 to April 2003. The study protocol was approved by the Institutional Review Board at the University of Minnesota, School of Medicine. Informed written consent was obtained prior to all studies. Patients were referred by medical oncologists working at the University of Minnesota or in private practice. Information collected for each patient included age, menopausal status, use of hormone replacement therapy, use of oral contraceptive pills, method of breast biopsy, diagnosis, ER (estrogen receptor)/PR (progesterone receptor) status, lesion size, and [tCho]. Each patient received the standard 4 doses of adriamycin and cyclophosphamide (AC) (doxorubicin — 60 mg/m^2, cyclophosphamide — 600 mg/m^2). The first dose of AC was given on day 1 and each additional dose of AC was given at 21-day intervals for a total of 64 days. Patients underwent MRI/MRS scans prior to treatment, within 24 hours after the first dose of AC was administered (day 2), and after the fourth dose of AC prior to surgery. Patients had the option of returning for additional scans after the second and third doses of AC. Patients received a baseline scan at a median of 2 days (range 1 to 21 days) prior to the first dose of AC and the final scan at a median of 3 days (range 1 to 8 days) after the fourth dose of AC. After completing 4

cycles of AC, one patient continued treatment with 4 cycles of paclitaxel and underwent additional scans after the second and fourth dose of paclitaxel.

MRI and MRS techniques

All measurements were performed with a 4T research scanner, consisting of a 90cm bore magnet (model 4T — 900, Oxford Magnet Technology, Oxford shire, UK) with a clinical gradient system (model 'Sonata', Siemens, Erlangen, Germany) interfaced with an imaging spectrometer (model 'Unity Inova', Varian, Palo Alto, CA). The gradient system was capable of 40mT/m with a 400μs rise time. Several different single-breast quadrature transmit/receive radio frequency (RF) surface coils of similar design were used to accommodate different breast sizes (26). The coils were mounted onto a custom-built patient table designed for unilateral, prone breast studies. Patients were positioned prone with their breast centered horizontally in the magnet. After acquiring scout images to verify proper positioning, the coil was manually tuned and matched. A high spatial resolution 3D fast low-angle shot (FLASH) image (fat-suppressed, matrix = 256 x 256 x 64, field of view = 14—18 cm, TR/TE = 13.5/4.1 ms, flip angle = 30°) and a fast 2D multislice FLASH image (fat-suppressed, matrix = 256 x 128, 30 slices, slice thickness = 2.5 mm, field of view = 14—18 cm, TR/TE = 390/5.1 ms, flip angle = 90°) were acquired prior to injection of Gd—DTPA (0.1 mmol/kg body weight). Five sets of 2D images were acquired immediately after injection, followed by a second 3D image acquisition. Both image sets were analyzed using our own image processing software (developed with Matlab; The Mathworks, Natick, MA) to select voxels for MRS with the subject still in the magnet.

Voxel placement was usually performed jointly by at least two of the authors (SM, PJB, EHB, and MG). In a few instances only the physician (SM or EHB) performed voxel placement, but only after having at least 6 months of experience in breast MR. Criteria for voxel selection included lesion architecture, lesion size ($\geq$ 2 cm in longest diameter), dynamic contrast uptake, and prior clinical information obtained from mammographic or ultrasound images. Voxels were planned to maximize coverage of the lesion while minimizing inclusion of adipose tissue. Voxels that were planned in studies following PST were placed to cover the same portion of the lesion covered in the baseline scan. If the lesion changed in size, the voxel was adjusted accordingly. Single-voxel ^{1}H spectroscopy was performed with the technique known as localization by adiabatic selective refocusing (LASER) (27). MRS data were acquired using 4096 complex points and 6 kHz spectral width. Each voxel measurement began with a calibration of the localized B_1 field strength, followed by 30—60 s of manual adjustment of the linear shims. A fully relaxed, single-shot, unsuppressed spectrum was acquired to measure the water and lipid signals. The RF power was then manually adjusted to suppress the water signal using the variable pulse power and optimized relaxation delays (VAPOR) technique (28). The metabolite spectrum was acquired using TE averaging with TE = 45—196 ms in 64 or 128 increments with TR=3 s (24). Each free induction decay signal was individually saved – no averaging was performed until processing. Levels of [tCho] were quantified by fitting a Voigt lineshape model to the data and using the unsuppressed water signal as an internal reference (25). All [tCho] measurements were recorded in units of mmol/kg water.

Data and Statistical Analysis

Statistical Analysis was done using the SAS software package system for Windows (version 8.02, Cary, North Carolina). Lesion size was measured from the high spatial resolution 3D subtraction image that was obtained by subtracting the baseline 3D image from the contrast-enhanced 3D image. The variable used to characterize lesion size was longest diameter (LD). LD measured at baseline and after the fourth dose of AC are represented by the variables LD_0 and LD_f respectively. Derived variables included LD after the fourth dose of AC normalized to baseline and expressed as a percentage,

$$\%LD_f = 100\left(\frac{LD_f}{LD_0}\right), \quad [1]$$

and the percent change in lesion size from baseline to after the fourth dose of AC,

$$\%\Delta LD_f = 100\left(\frac{(LD_f - LD_0)}{LD_0}\right). \quad [2]$$

Concentrations of tCho at baseline, within 24 hours after the first dose of AC, and after the fourth dose of AC are represented by the variables $[tCho]_0$, $[tCho]_{24}$, and $[tCho]_f$, respectively. Derived variables included the [tCho] at 24 hours normalized to baseline and expressed as a percentage,

$$\%[tCho]_{24} = 100\left(\frac{[tCho]_{24}}{[tCho]_0}\right), \quad [3]$$

and the percent change in [tCho] from baseline to 24 hours after the first dose of AC,

$$\%\Delta[tCho]_{24} = 100\left(\frac{[tCho]_{24} - [tCho]_0}{[tCho]_0}\right). \quad [4]$$

Using the classification system of the Response Evaluation Criteria in Solid Tumors (RECIST) (29), patients were categorized into one of two groups: objective responders or nonresponders. Objective responders were patients who had $\%\Delta LD_f \leq -30\%$. Nonresponders were patients who had $\%\Delta LD_f > -30\%$. The association between $\%\Delta[tCho]_{24}$ and $\%\Delta LD_f$ was calculated using Pearson's correlation coefficient (30). The comparison between $\%\Delta[tCho]_{24}$ and patient response, and the comparison of $[tCho]_0$ between objective responders and nonresponders, were calculated using the Wilcoxon rank-sum test (31).

Results

Patient and Tumor Characteristics

A total of 16 patients were recruited, of which 14 completed the protocol. Two patients did not complete the study because one opted to have surgery prior to completing all four doses of PST and the second patient decided to undergo an alternative method of treatment. Among the 14 patients who completed the study, 1 patient was not included in the data analysis due to an inability to plan a suitable voxel for [tCho] measurements. This patient was a 49 year-old female with inflammatory breast cancer (IBC). At baseline, the maximum width of the mass was only 0.3 cm, whereas LD_0 was 6 cm.

Table 1 lists the lesion size, [tCho], diagnosis, clinical response, and ER/PR status of the 13 patients who completed the protocol. The median age of the patient group was 46 years old (range 31 to 70 years). Of these 13 patients, eight were premenopausal of whom 5 had a prior history of taking oral contraceptives. Five patients were postmenopausal of whom 2 were on hormone replacement therapy. Histologic diagnosis

was obtained by ultrasound-guided needle core biopsy in 11 patients and by mammographic stereotactic-guided biopsy in 2 patients. Six patients were diagnosed with invasive ductal carcinoma (IDC) of whom 4 also had ductal carcinoma in situ (DCIS). Two patients were diagnosed with invasive lobular carcinoma (ILC) of whom 1 also had DCIS and the other also had both DCIS and lobular carcinoma in situ (LCIS). Four patients were diagnosed with IBC of whom 1 also had DCIS and another also had LCIS. One patient was diagnosed with both IDC and ILC. Eight patients were ER positive and 5 were PR positive. Three patients had additional breast lesions with $LD_0 < 2$ cm. Because these additional lesions did not fit the voxel selection criteria for MRS, they were not evaluated.

The median LD_0 was 3.8 cm (range 2.1 to 9.5 cm). The median LD_f was 2.7 cm (range 0 to 9.5 cm). The median $[tCho]_0$ was 4.5 mmol/kg (range 0.9 to 8.5 mmol/kg) for objective responders and 1.4 mmol/kg (range 0.8 to 2.3 mmol/kg) for nonresponders. Overall, $[tCho]_0$ was significantly higher for objective responders than for nonresponders (Wilcoxon rank-sum test, $p = 0.03$). The median $[tCho]_{24}$ was 3.4 mmol/kg (range 0 to 6.1 mmol/kg) for objective responders and 1.7 mmol/kg (range 0.8 to 3.4 mmol/kg) for nonresponders. The median $[tCho]_f$ was 0.5 mmol/kg (range 0 to 2.4 mmol/kg) for objective responders and 1.4 mmol/kg (range 0 to 3.0 mmol/kg) for nonresponders.

Objective Response

Eight of 13 patients experienced an objective response with diminished lesion size. The median $\%\Delta LD_f$ was -56% (range -35 to -100%), and the median $\%\Delta[tCho]_{24}$

was -30% (range -16 to -100%). All 8 patients who were objective responders had $[tCho]_0 > [tCho]_{24} \geq [tCho]_f$ (Table 1). Figure 1 shows $[tCho]_{24}$ and LD_f as a percent of the baseline for the objective responders.

Figure 2 shows MR data from an objective responder. At baseline, [tCho] was 4.6 mmol/kg and LD was 4.0 cm. Twenty-four hours after the first dose of AC was administered, [tCho] dropped to 3.7 mmol/kg whereas LD remained at 4.0 cm. At that point, $\%\Delta[tCho]_{24}$ was -20% and it was predicted that the patient would have an objective response. After the fourth dose of AC (day 64), [tCho] decreased to 0.9 mmol/kg and LD was 1.7 cm. Based on $\%\Delta LD_f$, which was -58%, the patient was classified as an objective responder. This patient had palpable lymphadenopathy. Since treatment with paclitaxel is regarded as standard therapy for node-positive patients (32), this patient was continued on systemic therapy with paclitaxel prior to surgery. Interestingly, 24 hours after the second dose of paclitaxel, [tCho] increased to 4.1 mmol/kg and LD remained at 1.7 cm. Although not shown in the figure, LD after the fourth dose of paclitaxel remained at 1.7 cm, whereas [tCho] increased to 4.8 mmol/kg.

No Response

Five of 13 patients were nonresponders. The median $\%\Delta LD_f$ was -13% (range 0 to -23%) and the median $\%\Delta[tCho]_{24}$ was 13% (range 0 to 50 %). All 5 patients who were nonresponders had a $[tCho]_0 \leq [tCho]_{24}$. With respect to $[tCho]_0$, $[tCho]_f$ was lower in 2 patients, higher in 2 patients, and the same in 1 patient (Table 1). Figure 3 shows $[tCho]_{24}$ and LD_f as a percent of the baseline for nonresponders.

Figure 4 shows MR data from a nonresponder. At baseline, [tCho] was 1.4 mmol/kg and LD was 2.9 cm. Twenty-four hours after the first dose of AC was administered, [tCho] increased to 2.1 mmol/kg whereas LD remained at 2.9 cm. At that point, $\%\Delta[tCho]_{24}$ was 50% and it was predicted that the patient would be a nonresponder. After the fourth dose of AC (day 65), [tCho] was 0.9 mmol/kg and LD was 2.7 cm. Based on $\%\Delta LD_f$ of only -7%, this patient was classified as a nonresponder.

Correlation between $\%\Delta[tCho]_{24}$ and $\%\Delta LD_f$

A significant positive correlation between $\%\Delta[tCho]_{24}$ and $\%\Delta LD_f$ was found ($R = 0.79$, $p = 0.001$). Figure 5 shows a graph of the correlation between $\%\Delta[tCho]_{24}$ and $\%\Delta LD_f$. Different symbols were used to indicate the group into which each patient was categorized: objective responder or nonresponder, based on the RECIST criteria. All 5 patients who were nonresponders (black squares) had a $\%\Delta[tCho]_{24} \geq 0$. All 8 patients who had an objective response (white squares) had a $\%\Delta[tCho]_{24} < 0$. $\%\Delta[tCho]_{24}$ was significantly different between objective responders and nonresponders (Wilcoxon rank-sum test, $p = 0.007$).

Discussion

This pilot study shows that ^1H MRS appears to predict clinical response in patients with locally advanced breast cancer within 24 hours of receiving the first dose of primary systemic therapy. These results suggest that the addition of high field ^1H MRS can offer a substantial advantage over using MRI alone in predicting response to PST.

Overall, patients who were objective responders had a higher $[tCho]_0$ when compared to patients who were nonresponders. All patients who were objective responders had a lower $[tCho]_{24}$ as compared to $[tCho]_0$, and in lesions with measurable $[tCho]_{24}$, a further decrease in [tCho] was observed after the fourth dose of AC. Perhaps the immediate decrease in [tCho] within 24 hours after the first dose of AC reflects inhibition of cellular proliferation and the acute cytotoxic effect of chemotherapy. All patients who were nonresponders had either no change or a higher $[tCho]_{24}$ as compared to $[tCho]_0$. This may be related to the fact that certain breast neoplasms exhibit *de novo* resistance to chemotherapy and as a result, PST with the AC regimen would have no effect on the proliferating neoplastic cells.

It is expected that quantitative ^1H MRS will not only improve the accuracy of MRI in detecting breast cancer, but as shown here, it may be used with MRI to assess response to PST early in the course of treatment. Similar to our study, one group of researchers found that within a majority of patients who underwent PST for breast cancer, there was a disappearance or a decrease in tCho signal (21). However, this earlier study did not categorize which patients had a change in tCho signal nor did it describe when the change in signal occurred. In a study using ^1H MRS to evaluate treatment response in pediatric gliomas, the ratio of tCho signals from tumor and normal white matter was measured (23). In brain tumors that responded clinically, there was a decrease in the tCho ratio, whereas in patients who did not respond, there was no change or an increase in the tCho ratio.

The precise mechanism(s) as to why neoplastic tissues exhibit elevated tCho levels still remains unanswered. It has been proposed that increased phosphocholine, the primary metabolite responsible for the tCho peak in neoplastic tissue, is a result of increased synthesis of membranes by replicating cells. Elevated tCho may reflect a change in the balance between biosynthetic and catabolic pathways in which choline compounds serve as both precursors and catabolites (33). Other researchers have observed that the predominant intracellular mechanism responsible for the augmented levels of phosphocholine is due to up-regulation of choline kinase (34).

Although no PST regimen other than AC was considered in this study, it is interesting to note the pattern of change in [tCho] for the patient who continued treatment with 4 doses of paclitaxel prior to surgery. Despite the fact that this individual was an objective responder to AC, the patient did not respond to paclitaxel. Between the last dose of AC and the second dose of paclitaxel, the patient's [tCho] increased by 355%, from 0.9 to 4.1 mmol/kg, whereas the lesion size did not change. The patient's lesion size, even after the fourth dose of paclitaxel, remained at 1.7 cm, while the [tCho] increased further by 17%, from 4.1 to 4.8 mmol/kg. It is reasonable to assume that early changes seen in ^{1}H MRS may even be used in predicting clinical response between different regimens. Although the findings of this study showed that $\%\Delta[tCho]_{24}$ was an early marker for response to the specific cytotoxic agent AC, further work is needed to determine whether early prediction is possible with other agents.

Among all objective responders in our study, the smallest change in [tCho] within 24 hours was a decrease of 16%. The ability to predict response depends on having sufficient accuracy and reproducibility in the MRS measurement, and thus future studies using multiple baseline scans are needed to establish the variance of [tCho] measurements. We believe the accuracy of a [tCho] measurement is limited primarily by signal-to-noise ratio (SNR) which has been shown to increase at least linearly with magnetic field strength (35, 36). Thus, the 4T scanner used here offered a significant advantage over 1.5T. Further studies are needed to determine whether 1.5T scanners can provide the SNR necessary to measure [tCho] accurately. However, newer 3T clinical scanners are expected to perform similarly to the 4T research scanner used here. An additional limitation of MRS is the inability to predict clinical response in breast cancers that are small, diffuse, or irregularly shaped. Due to SNR limitations, [tCho] in voxels < 1 cm^3 may be difficult to measure accurately. Fortunately, the minimum voxel size used for monitoring response to PST will typically be greater than 1 cm^3, since tumors must be at least 2 cm in LD (Stage II or higher) to be eligible for PST by current criteria. Breast tumors with thin or linear morphology can pose a problem for the spectroscopist planning the voxel, particularly when intense lipid signals are contained in the voxel (24). For example, data from one patient were excluded from the analysis due to an inability to plan a suitable voxel for [tCho] measurements at baseline and following PST. At baseline, the MRI revealed a diffuse, linearly shaped mass. Due to the thin conformation of this lesion, it was not possible to place a rectangular voxel containing less than 33% fat by volume, as required by the quantification method (25).

The observation of consistent trends in the $\%\Delta[tCho]_{24}$ between objective responders and nonresponders suggests that *in vivo* ^{1}H MRS, with MRI, may be a sensitive indicator in predicting clinical response as early as 24 hours after the first dose of PST. Monitoring patients on PST with MRS appears to offer a means to detect the presence of viable and/or proliferating neoplastic cells. With the possibility of early prediction comes the benefit of immediate assessment in tailoring an effective regimen for individual patients. Perhaps early changes seen in ^{1}H MRS scans of patients who undergo PST may even serve as an indicator of risk for recurrent or metastatic breast cancer. Furthermore, the opportunity for such early prediction will be useful to researchers seeking to evaluate new PST drugs and may help to elucidate the mechanisms of multi-drug resistance in breast cancer.

These promising findings were obtained from a small group of patients and thus a study of a larger prospective patient series is needed. A larger study may also provide information about the possibility of using MRS to predict when a patient is destined to have a pathologic complete response. To the best of our knowledge, this is the first report in which quantitative tCho measurements were made with *in vivo* ^{1}H MRS for the purpose of predicting clinical response to PST in breast cancer.

Acknowledgements

The authors are grateful to Ms. Bibi Husain, Lou Forsythe, R.N., Julliette Gay, R.N., Susan Pappas-Varco, R.N., and the General Clinical Research Center nursing staff for their help in coordinating the study. We thank Joseph Leach, M.D. and Amy Spomer, M.D. for referring patients. We are also grateful to Joseph Lin, Ph.D., Bridget Sestero, M.D., Ms. Ann Musgjerd, and Ryan Chamberlain, B.S. for their efforts in gathering data and helping with the study.

This research was supported by DOD Breast Cancer Research Program DAMD 17-01-1-0331, NIH grants RR08079, CA92004, RR00400, and PHS Cancer Center Support Grant P30 CA77398, the Lillian Quist-Joyce Henline Chair in Biomedical Research, and the Tickle Family Land Grant Chair in Breast Cancer Research.

References

1. Fisher B, Brown A, Mamounas E, et al. Effect of preoperative chemotherapy on local-regional disease in women with operable breast cancer: Findings from national surgical adjuvant breast and bowel project B-18. J Clin Oncol 1997; 15:2483-2493.
2. Fisher B, Bryant J, Wolmark N, et al. Effect of preoperative chemotherapy on outcome of women with operable breast cancer. J Clin Oncol 1998; 16:2672-2685.
3. Smith IC, Heys SD, Hutcheon AW, et al. Neoadjuvant chemotherapy in breast cancer: significantly enhanced response with docetaxel. J Clin Oncol 2002; 20:1456-1466.
4. Kaufmann M, Von Minckwitz G, Smith R, et al. International expert panel on the use of primary (preoperative) systemic treatment of operable breast cancer: review and recommendations. J Clin Oncol 2003; 21:2600-2608.
5. Junkerman H, Founier D. Imaging procedures for assessment of the response of mammary carcinoma to preoperative chemotherapy. Radiologe 1997; 37:726-732.
6. Segel MC, Paulus DD, Hortobagyi GN. Advanced primary breast cancer: assessment at mammography response to induction chemotherapy. Radiology 1988; 169:49-54.
7. Vinnicombe SJ, Mac Vicar AD, Guy RL, Sloane JP, Powles TJ, Knee G, Husband JE. Primary breast cancer: mammographic changes after neoadjuvant chemotherapy, with pathologic correlation. Radiology 1996; 198:333-340.

8. Herrada J, Iyer RB, Atkinson EN, Sneige N, Buzdar AU, Hortobabyi GN. Relative value of physical examination, mammography, and breast sonography in evaluating the size of the primary tumor and regional lymph node metastases in women receiving neo-adjuvant chemotherapy for locally advanced breast carcinoma. Clin Cancer Res 1997; 3:1565-1569.
9. Esserman L, Kaplan E, Partridge S, et al. MRI phenotype is associated with response to doxorubicin and cyclophosphamide neoadjuvant chemotherapy in stage III breast cancer. Ann Surg Oncol 2001; 8:549-559.
10. Gilles R, Guinebretiere JM, Toussaint C, et al. Locally advanced breast cancer: contrast-enhanced subtraction MR imaging of response to preoperative neoadjuvant chemotherapy. Radiology 1994; 191:633-638.
11. Abraham DC, Jones RC, Jones SE, et al. Evaluation of neoadjuvant chemotherapeutic response of locally advanced breast cancer by magnetic resonance imaging. Cancer 1996; 78:91-100.
12. Balu-Maestro C, Chapellier C, Bluese A, Chanalet I, Chauvel C, Largillier R. Imaging in evaluation of response to neoadjuvant breast cancer treatment benefits of MRI. Breast Cancer Res Treat 2002; 72:145-152.
13. Rieber A, Brambs HJ, Gabelmann A, Heilmann V, Kreienberg R, Kühn T. Breast MRI for monitoring response of primary breast cancer to neo-adjuvant chemotherapy. Eur Radiol 2002; 12:1711-1719.
14. Choyke PL, Dwyer AJ, Knopp MV. Functional tumor imaging with dynamic contrast-enhanced magnetic resonance imaging. J Magn Reson Imaging 2003; 17:509-520.

15. Delille J, Slanetz PJ, Yeh ED, Halpern EF, Kopans DB, Garrido L. Invasive ductal breast carcinoma response to neoadjuvant chemotherapy: Noninvasive monitoring with functional MR imaging-pilot study. Radiology 2003; 228:63-69.

16. Mackinnon WB, Barry PA, Malycha PL, et al. Fine-needle biopsy specimens of benign breast lesions distinguished from invasive cancer ex vivo with proton MR spectroscopy. Radiology 1997; 204:661-666.

17. Roebuck JR, Cecil KM, Schnall MD, Lenkinski RE. Human breast lesions: Characterization with proton MR spectroscopy. Radiology 1998; 209: 269-275.

18. Gribbestad IS, Sitter B, Lundgren S, Krane J, Axelson D. Metabolite composition in breast tumors examined by proton nuclear magnetic resonance spectroscopy. Anticancer Res 1999; 19:1737-1746.

19. Kvistad KA, Bakken IJ, Gribbestad IS, et al. Characterization of neoplastic and normal human breast tissues with *in vivo* ^{1}H NMR spectra with increased magnetic field strength. J Magn Reson Imaging 1999; 10:159-164.

20. Katz-Brull R, Lavin PT, Lenkinski R. Clinical utility of proton magnetic resonance spectroscopy in characterizing breast lesions. J Natl Cancer Inst 2002; 94: 1197-1203.

21. Jagannathan NR, Kumar M, Seenu V, et al. Evaluation of total choline from *in-vivo* volume localized proton MR spectroscopy and its response to neoadjuvant chemotherapy in locally advanced breast cancer. Br J Cancer 2001; 84:1016-1022.

22. Schwarz AJ, Maisey NR, Collins DJ, Cunningham D, Huddart R, Leach MO. Early *in vivo* detection of metabolic response: a pilot study of ^{1}H MR

spectroscopy in extracranial lymphoma and germ cell tumours. Br J Radiol 2002; 75:959-966.

23. Lazareff JA, Gupta RK, Alger J. Variation of post-treatment ^{1}H-MRSI choline intensity in pediatric gliomas. J Neurooncol 1999; 41:291-298.
24. Bolan PJ, DelaBarre L, Baker EH, et al. Eliminating spurious lipid sidebands in ^{1}H MRS of breast lesions. Magn Reson Med 2002; 48:215-222.
25. Bolan PJ, Meisamy S, Baker EH, et al. *In vivo* quantification of choline compounds in the breast with ^{1}H MR Spectroscopy. Magn Reson Med 2003; 50: 1134-1143.
26. Merkle H, DelaBarre L, Bolan PJ, et al. Transceive quadrature breast coils and applications at 4 Tesla (abstr). In: Proceedings of the 9th Annual Meeting of the International Society for Magnetic Resonance in Medicine. Glasgow, Scotland: International Society for Magnetic Resonance in Medicine, 2001; 1114.
27. Garwood M, DelaBarre L. The return of the frequency sweep: designing adiabatic pulses for contemporary NMR. J Magn Reson 2001; 153:155-177.
28. Tkac I, Starcuk Z, Choi IY, Gruetter R. *In vivo* ^{1}H NMR spectroscopy of rat brain at 1 msec echo time. Magn Reson Med 1999; 41:649-656.
29. Therasse P, Arbuck SG, Eisenhauer EA, et al. New guidelines to evaluate the response to treatment in solid tumors. European organization for research and treatment of cancer, National Cancer Institute of the United States, National Cancer Institute of Canada. J Natl Cancer Inst 2000; 92:205-216.
30. Le CT. Descriptive methods for continuous data. Introductory Biostatistics. Hoboken, NJ: John Wiley & Sons, Inc., 2003; 85-88.

31. Le CT. Comparison of population means. Introductory Biostatistics. Hoboken, NJ: John Wiley & Sons, Inc., 2003; 246-281.

32. Henderson IC, Berry DA, Demetri GD, et al. Improved outcomes for adding sequential paclitaxel but not from escalating doxorubicin dose in an adjuvant chemotherapy regimen for patients with node-positive primary breast cancer. J Clin Oncol 2003; 21:976-983.

33. Podo F. Tumour phospholipid metabolism. NMR Biomed 1999; 12:413-439.

34. Degani H, Rushkin E, Eliyahu G. Variations in the augmentation of phosphocholine in breast cancer; the cause and the sense (abstr). In: Proceedings of the 11th Annual Meeting of the International Society for Magnetic Resonance in Medicine. Toronto, Ontario, Canada: International Society for Magnetic Resonance in Medicine, 2003; 1280.

35. Vaughan JT, Garwood M, Collins CM, et al. 7T vs. 4T: RF power, homogeneity, and signal-to-noise comparison in head images. Magn Reson Med 2001; 46:24-30

36. Hoult DI, Richard RE. The signal-to-noise ratio of the nuclear magnetic resonance experiment. J Magn Reson 1976; 24:71-85.

Table 1

Patient No	LD_0 (cm)	LD_f (cm)	$[tCho]_0$ (mmol/kg)	$[tCho]_{24}$ (mmol/kg)	$[tCho]_f$ (mmol/kg)	Diagnosis	Clinical Response	ER/PR
1	4.0	1.7	4.6	3.7	1.0	IDC/DCIS	OR	+/-
2	6.8	3.3	1.7	0.9	0.6	ILC/DCIS	OR	+/-
3	9.3	4.2	7.8	5.4	2.4	IBC	OR	-/+
4	2.8	0	2.7	0	0	IDC/DCIS	OR	+/+
5	3.1	0.8	0.9	0.7	0	IDC	OR	-/-
6	2.1	1.0	4.5	3.0	0.4	ILC/LCIS/DCIS	OR	+/+
7 †	2.3	0.7	4.5	3.8	0	IDC/DCIS	OR	-/+
8	4.8	3.1	8.5	6.1	1.2	IDC/DCIS	OR	+/-
9	9.5	9.5	1.1	1.1	0.3	IBC/DCIS	NR	-/-
10	2.9	2.7	1.4	2.1	1.4	IDC	NR	-/-
11 †	3.8	3.3	0.8	0.8	0	IDC/ILC	NR	+/+
12	2.5	2.0	1.5	1.7	2.5	IBC/LCIS	NR	+/-
13 †	4.7	3.6	2.3	3.4	3.0	IBC	NR	+/-

LD_0 = lesion size at baseline, LD_f = lesion size after the fourth dose of AC, $[tCho]_0$ = total choline concentration at baseline, $[tCho]_{24}$ = total choline concentration within 24 hours after the first dose of AC, $[tCho]_f$ = total choline concentration after the fourth dose of AC, IDC = invasive ductal carcinoma, ILC = invasive lobular carcinoma, IBC = inflammatory breast cancer, DCIS = ductal carcinoma in situ, LCIS = lobular carcinoma in situ, OR = objective response, NR = no response, ER = estrogen receptor, PR = progesterone receptor, + = positive, - = negative, † = patients with additional satellite lesions less than 2 cm in longest diameter that did not fit the inclusion criteria for MRS measurements.

Figure Captions

Figure 1 – The effects of treatment on the concentration of choline-containing compounds ([tCho]) and lesion size (LD) in patients with an objective response. The dashed line represents the normalized value of [tCho] and LD at baseline. The diamonds represent [tCho] at 24 hours after the first dose of AC normalized to baseline and expressed as a percentage ($\%[tCho]_{24}$) and the circles represent LD after the fourth dose of AC normalized to baseline and expressed as a percentage ($\%LD_f$). $\%[tCho]_{24}$ and $\%LD_f$ pairs from individual subjects are indicated by connecting lines. Notice that all the objective responders had a $[tCho]_{24}$ that was less than [tCho] at baseline.

Figure 2 – MRI and MRS of a patient with an objective response to AC. The patient was a 43 year-old female who was diagnosed with invasive ductal carcinoma with positive lymph nodes. Images of the right breast (sagittal view) were acquired at 7 minutes post Gd-DTPA injection using fat-suppressed 3D FLASH (13.5/4.1). The box surrounding the enhancing lesion depicts the MRS voxel. Corresponding spectra are shown to the right. The spectral peaks labeled 1-3 in (a) arise from lipid, tCho, and water, respectively. The lines above and below the tCho peak represent the fitted tCho peak and the residual of the fit, respectively. (a) Two days prior to starting AC, tCho concentration ($[tCho]_0$) = 4.6 mmol/kg and lesion size (LD_0) = 4.0 cm. (b) Within 24 hrs after the first dose of AC, tCho concentration ($[tCho]_{24}$) = 3.7 mmol/kg and lesion size (LD) = 4.0 cm. (c) After the fourth dose of AC, tCho concentration ($[tCho]_f$) = 0.9 mmol/kg and lesion size (LD_f) = 1.7 cm. (d) After the second dose of paclitaxel, [tCho] = 4.1 mmol/kg and LD = 1.7 cm. Using equation 4, the percent change in tCho concentration ($\%\Delta[tCho]_{24}$) was -20%,

predicting an objective response to AC. Using equation 2, the percent change in lesion size ($\%\Delta LD_f$) was -58%, compatible with an objective response to AC.

Figure 3 - The effects of treatment on the concentration of choline-containing compounds ([tCho]) and lesion size (LD) in nonresponders. The dashed line represents the normalized value of [tCho] and LD at baseline. The diamonds represent [tCho] at 24 hours after the first dose of AC normalized to baseline and expressed as a percentage ($\%[tCho]_{24}$) and the circles represent LD after the fourth dose of AC normalized to baseline and expressed as a percentage ($\%LD_f$). $\%[tCho]_{24}$ and $\%LD_f$ pairs from individual subjects are indicated by connecting lines. Notice that all the nonresponding patients had a $[tCho]_{24}$ which was greater than or equal to [tCho] at baseline.

Figure 4 – MRI and MRS of a nonresponding patient. The patient was a 42 year-old female who was diagnosed with invasive ductal carcinoma. Images of the right breast (sagittal view) were acquired at 7 minutes post Gd-DTPA injection using fat-suppressed 3D FLASH (13.5/4.1). The box surrounding the enhancing lesion depicts the MRS voxel. Corresponding spectra are shown to the right. The spectral peaks labeled 1-3 in (a) arise from lipid, tCho, and water, respectively. The lines above and below the tCho peak represent the fitted tCho peak and the residual of the fit, respectively. (a) One day prior to starting AC, tCho concentration ($[tCho]_0$) = 1.4 mmol/kg and lesion size (LD_0) = 2.9 cm. (b) Within 24 hrs after the first dose of AC, tCho concentration ($[tCho]_{24}$) = 2.1 mmol/kg and lesion size (LD) = 2.9 cm. (c) After the fourth dose of AC, tCho concentration ($[tCho]_f$) = 0.9 mmol/kg and lesion size after the fourth dose of AC (LD_f) = 2.7 cm.

Using equation 4, the percent change in tCho concentration ($\%\Delta[tCho]_{24}$) was 50%, predicting no response to AC. Using equation 2, the percent change in lesion size ($\%\Delta LD_f$) was -7%, compatible with a nonresponder to AC.

Figure 5 – Correlation between percent change in tCho concentration within 24 hours of the first dose of AC ($\%\Delta[tCho]_{24}$) and percent change in lesion size after the fourth dose of AC ($\%\Delta LD_f$). Each solid white square represents one of the 8 objective responding patients and each solid black square represents one of the 5 nonresponding patients. There is a statistically significant positive correlation between $\%\Delta[tCho]_{24}$ and $\%\Delta LD_f$, ($R = 0.79$, $p = 0.001$).

Figure 1

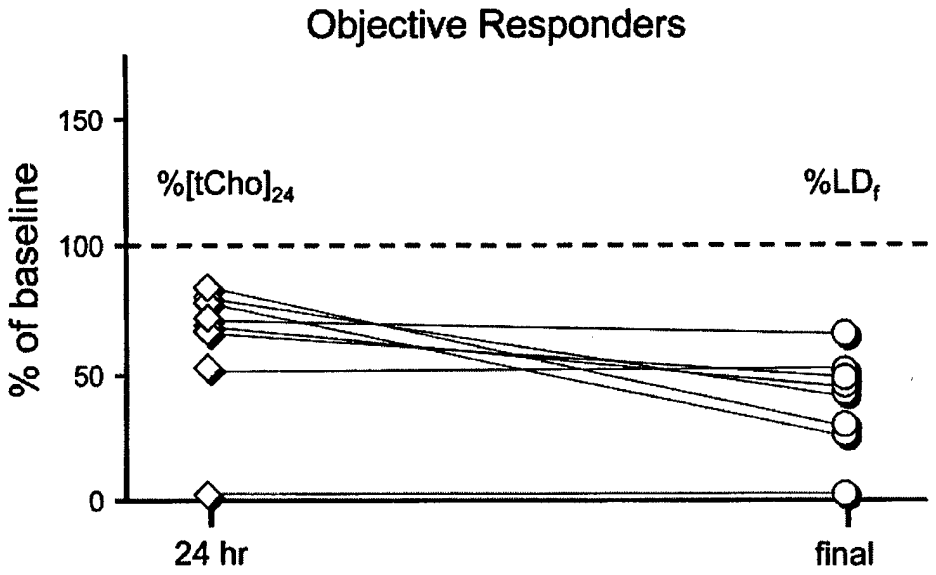
Objective Responders
150
100
50
0
% of baseline
%[tCho]24
%LDf
24 hr
final

Figure 2

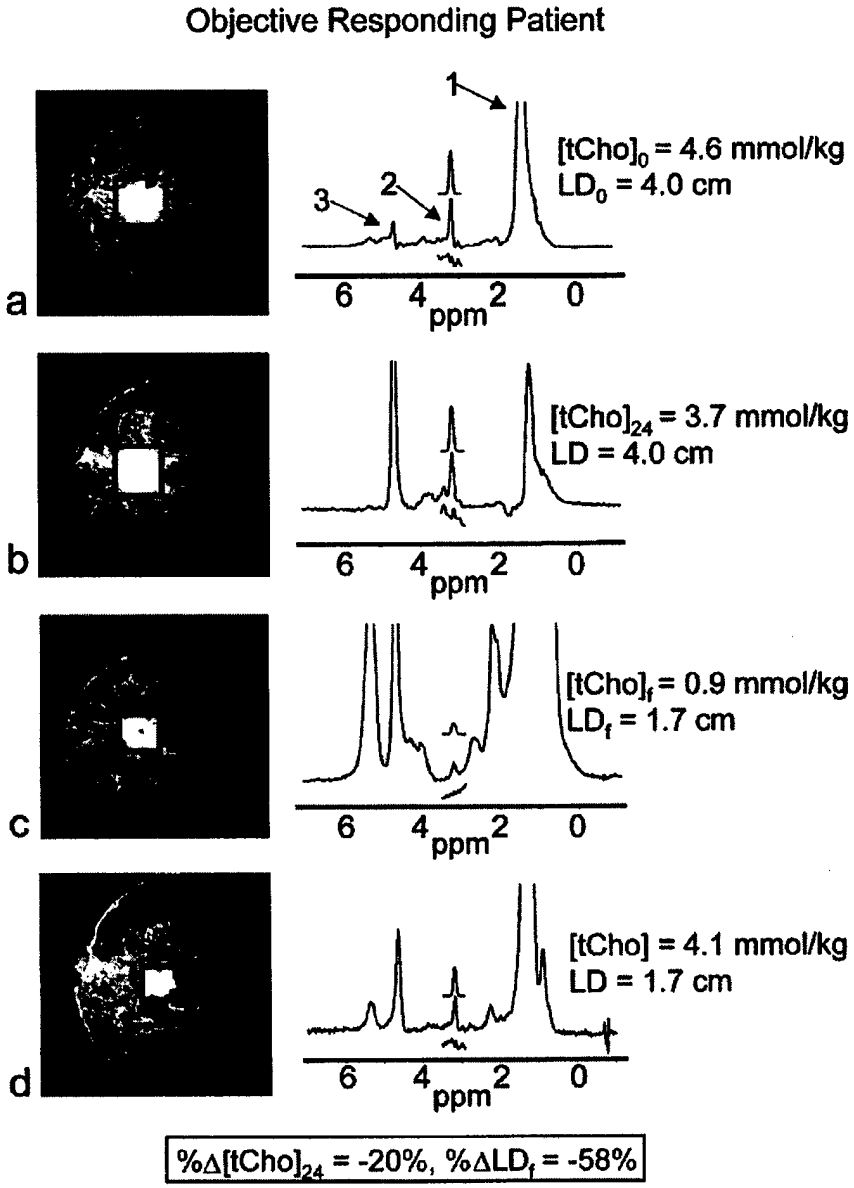
Objective Responding Patient
1
2
3
[tCho]0 = 4.6 mmol/kg
LD0 = 4.0 cm
a
6 4 ppm 2 0
[tCho]24 = 3.7 mmol/kg
LD = 4.0 cm
b
6 4 ppm 2 0
[tCho]f = 0.9 mmol/kg
LDf = 1.7 cm
c
6 4 ppm 2 0
[tCho] = 4.1 mmol/kg
LD = 1.7 cm
d
6 4 ppm 2 0
%Δ[tCho]24 = -20%, %ΔLDf = -58%

Figure 3

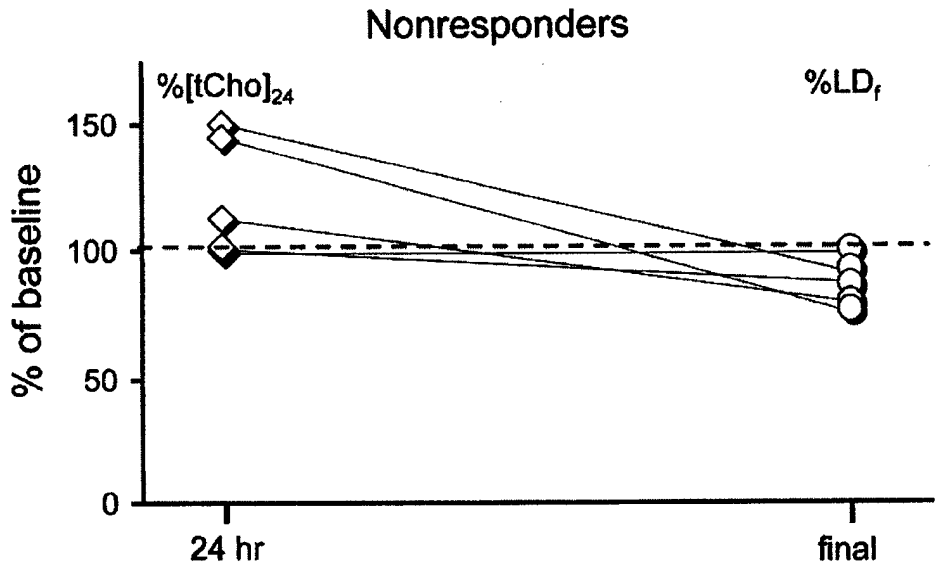
Nonresponders
%[tCho]24
%LDf
150
100
50
0
% of baseline
24 hr
final

Figure 4

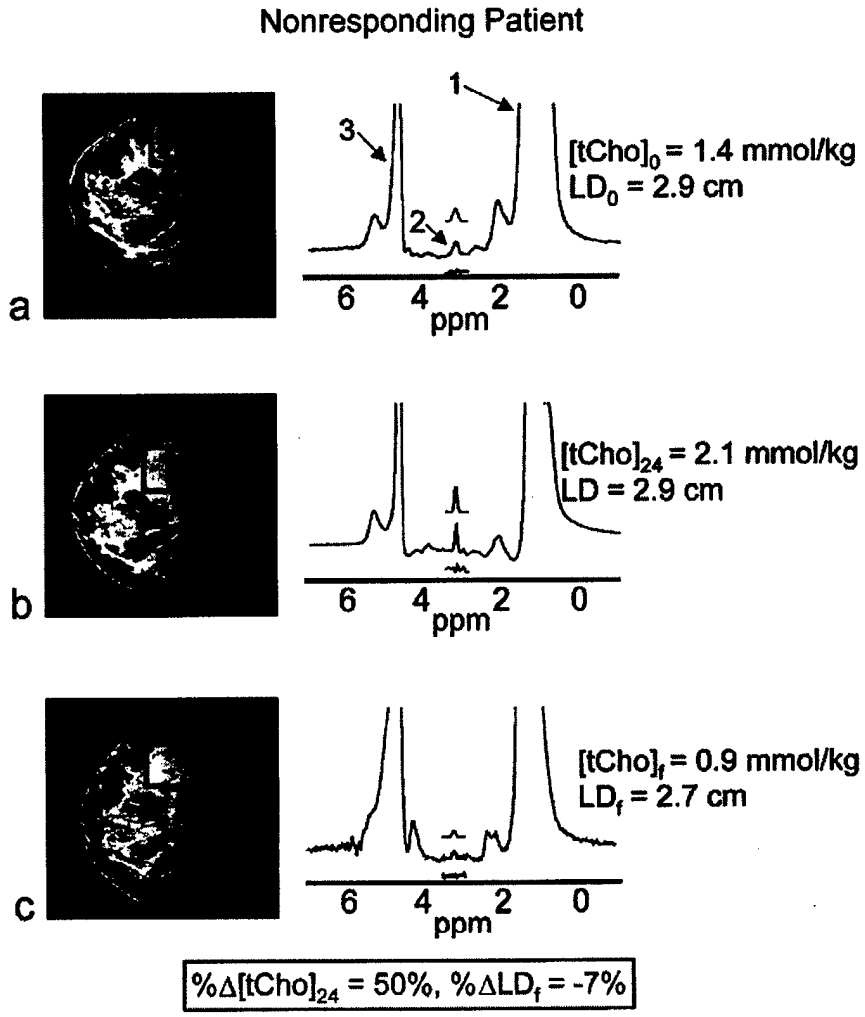
Nonresponding Patient
a
b
c
1
2
3
6
4
2
0
ppm
[tCho]0 = 1.4 mmol/kg
LD0 = 2.9 cm
[tCho]24 = 2.1 mmol/kg
LD = 2.9 cm
[tCho]f = 0.9 mmol/kg
LDf = 2.7 cm
%Δ[tCho]24 = 50%, %ΔLDf = -7%

Figure 5

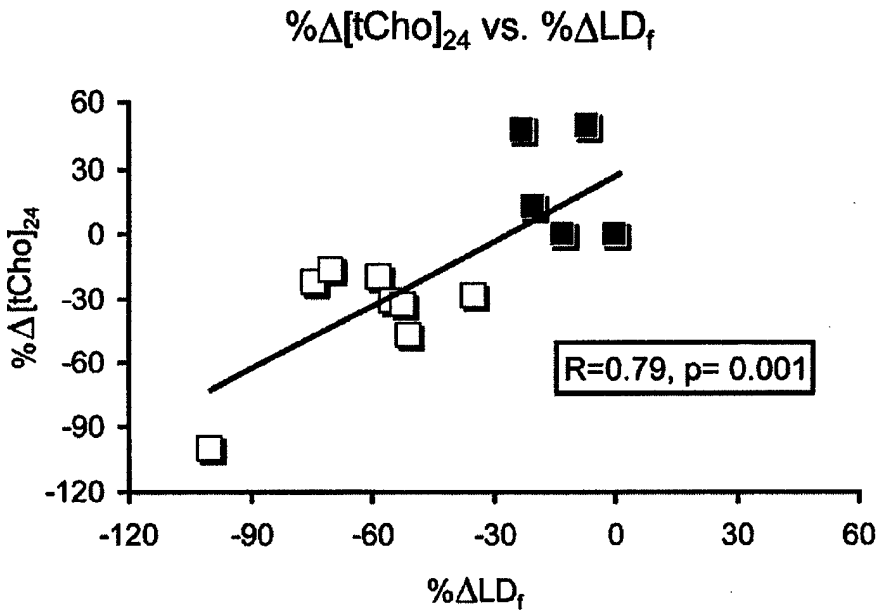
%Δ[tCho]24 vs. %ΔLDf
60
30
0
-30
-60
-90
-120
%Δ [tCho]24
-120
-90
-60
-30
0
30
60
%ΔLDf
R=0.79, p= 0.001